GEM TN-92-101
PDT-BU-92-8

Study of Hadron Punchthrough and Muon Rates at the SSC

Yuan-Hann Chang - Massachusetts Institute of Technology
B. Zhou - Boston University

May 1992

Abstract:

Hadron punchthrough probabilities functions of hadron energy and absorber length at the SSC are studied in detail. Energy spectra, charged multiplicity and the angular spread distributions of the punchthrough are presented. Total muon rates are calculated for the GEM detector baseline design.

GEM MEMO
PDT-BU-92-8

Study of Hadron Punchthrough and Muon Rates at the SSC

Yuan-Hann Chang* and B. Zhou**

)M.I.T. and *)Boston University**

May, 1992

Abstract:

Hadron punchthrough probabilities functions of hadron energy and absorber length at the SSC are studied in detail. Energy spectra, charged multiplicity and the angular spread distributions of the punchthrough are presented. Total muon rates are calculated for the GEM detector baseline design.

Study of Hadron Punchthrough and Muon Rates at the SSC

Yuan-Hann Chang
Physics Dept., M.I.T., Cambridge, MA 01239

Bing Zhou
Physics Dept., Boston University, Boston, MA 02215

Oct., 1991

ABSTRACT

Hadron punchthrough probabilities as functions of hadron energy and absorber length (in terms of interaction length) at the SSC are studied in detail using GEANT Monte Carlo simulations. Energy spectra, charged multiplicity and the angular spread distributions of the punchthroughs are presented. Total muon rates including prompt muons and the punchthroughs are calculated as functions of muon transverse momentum and the rapidity coverage with GEM detector baseline design.

1 Introduction

Experiments at the next generation of hadron colliders (SSC/LHC), operating at very high luminosities ($10^{33} - 10^{34} cm^{-2} s^{-1}$), will allow us to explore the physics behind the electroweak symmetry breaking. This implies the search for the Higgs boson, technicolor, supersymmetry, as well as the search for new gauge bosons, new leptons and quarks. Leptonic/photonic final states will be detected as the most sensetive signatures for new physics. At the extremely high luminosities, muons offer an advantage over electrons/photons since the trigger and the measurement can be performed outside of the calorimeters (as absorbers of hadrons), where the particle

flux is low. For high luminosity hadron colliders, muon detections is therefore the first principle in optimizing the detector design.

Very broad physics topics at the TeV energy scale require the muon detection at the SSC to cover large range of the muon momentum, from few GeV to few TeV, and large solid angle, down to few degrees (rapidity larger than 2.5). Understanding the hadron punchthroughs and muon rates is crucial for muon detector and trigger design. However, punchthrough simulations need enormouse amount of computer time: in order to obtain reasonablly good spectra, we need to simulate in total about 13 million shower developments in the calorimeters. Our strategy for the simulations is therefore:

(1) To obtain punchthrough probabilities for single hadron (mainly pions) with different energies and incident angles (therefore different calorimeter thickness) using full GEANT[1] simulations;

(2) The total hit distributions in muon chambers and the muon trigger rates are obtained using ISAJET[2] Monte Carlo program to generate pp collision events. The punchthrough probabilities and the muon energy loss were then for each μ, π and k according to the spectra obtained from the GEANT simulations.

It is the goal of this study to provide detailed information on punchthroughs which should be easily used for total muon rate calculations of any detector configuration for high luminosity hadron colliders. We have used this information and calculated total muon rate with the GEM detector baseline design.

In this paper we will first describe the main parameters of the detector model and the physics processes set for hadronic shower simulation in GEANT programs. In section three we will report the results on simulations of single muon and pion with different energies and incidence angles. Section four reports the results of total muon rate calculations with GEM detector at the SSC. Discussions on the calculation uncertainties and the conclusions will be given in the last section.

2 Detector and Physics Parameters for GEANT Simulation

We have used a simplified detector model for GEANT (version 3.14), which uses the GHEISHA[3] collision model for a full shower simulations. Figure 1 shows the detector geometry set up:

(1) 1.5 mm Berillium beam pipe located at a distance(R) of 10 cm from the beam line:

(2) A simple Silicon central tracker from R=13-75 cm, with length=300 cm:

(3) BaF_2 EM calorimeters from R=78-130 cm in barrel, Z=210-262 cm in endcaps. It has in total 25 radiation lengths (X_0), corresponding to 1.7 interaction lengths (λ);

(4) Fe/Pb/scintillator sandwitch hadron calorimeter located between R=145-335 cm in the barrel, and Z=330-558 cm in the endcaps. Its total interaction length equals to 10.1λ in the barrel ($|\eta| < 1.1$), and 12.3λ in the endcaps.

(5) Three layers of Aluminum muon chambers located at R=370, 600, 830 cm in the barrel, Z=600, 1025, 1450 in the endcaps. Inner and outer chambers have 10% radiation length, and the middle chamber has 20% radiation length.

(6) All the subsystem detectors are located in a large magnetic field (1.0 T) with the field direction along the beam line.

Table 1 lists the values of the particle energy cutoff and the physics processes setup in the GEANT program to control the shower development and the tracking of the secondary particles in the detector.

3 Results from GEANT Simulations

Table 1: **Parameters used in GEANT Monte Carlo Simulations**

```
***** G E A N T     Version 3.1416        DATE/TIME 911005/2008 ******
*************************************************************
*                                                           *
*              Standard TPAR for this run are               *
*              ------------------------------               *
*                                                           *
*  CUTGAM=   1.00 GEV  CUTELE=   1.00 GEV  CUTNEU=   1.00 GEV *
*  CUTHAD=500.00 MEV  CUTMUO=100.00 MEV                     *
*  BCUTE =   1.00 GEV  BCUTM =   1.00 GEV                   *
*  DCUTE =   1.00 GEV  DCUTM =   1.00 GEV  PPCUTM= 10.00 MEV *
*  IPAIR =        1.   ICOMP =        1.   IPHOT =        1. *
*  IPFIS =        1.   IDRAY =        1.   IANNI =        1. *
*  IBREM =        1.   IHADR =        1.   IMUNU =        1. *
*  IDCAY =        1.   ILOSS =        1.   IMULS =        1. *
*  IRAYL =        0.                                         *
*                                                           *
*************************************************************
```

3.1 Hadron Punchthrough Probabilities

To obtain the punchthrough probabiliteis, we simulated the shower development of single pions and kaons incidented to the detectors from the interaction point. We have parallelly used about 10 VAX workstations, 2 DEC-5000 workstations and 10 SGI CPUs to run the computing jobs for about 6 weeks to study the hadron punchthroughs using GEANT full shower simulations. Table 2 lists number of hadron showers simulated in our studies.

In the following, we present main results which are needed for total muon rate calculations:

- **Single π^+ punchthrough probability:** It is defined as N_{out}/N_{total} where N_{out} is the number of events with charged particles leaking out of the calorimetry and N_{total} is the total number of pions simulated. N_{out}/N_{total} versus pion energies at several different interation lengthes are shown in Figure 2. π^- and $k^{\pm}$

punchthrough probilities at 90 degrees are compared with π^+ in Figure 3.

- **Single pion punchthrough charged multiplicity:** It is defined as the number of hits in the inner layer of the muon chambers from a single incident pion. Note that if a low energy particle loops in the magnetic field and hits the chamber twice, we have counted it twice. Figure 4 shows single pion punchthrough charged multiplicities at different pion energies and calorimetry thickness (in terms of λ).

- **Normalized momentum spectra:** It is defined as $p_{out}/p_{incident}$, where p_{out} is the momentum of the punchthrough particle and $p_{incident}$ is the momentum of the incident particle. For leading energy punchthrough charged particles the spectrum is shown in Figure 5. Figure 6 and Figure 7 show the spectra for the second and the third leading energy punchthrough particles, respectively. The spectra of low $p_{incident}$ at large λ show clear enhancement at high $p_{out}/p_{incident}$ values. These are contributions from the flight decays.

- **Punchthrough particle angular spread:** It is defined as the angles between the out-going punchthrough particles and the incident hadron. The angular spread is correlated to the normalized momentum. Figure 8 shows 2-dimension histograms, $\Delta\theta$ versus $p_{out}/p_{incident}$, for different incident pion energies.

3.2 Muon Energy Loss Spectra

The purpose to study muon energy loss in the calorimeters is:

(1) To obtain correct prompt muon spectra out of the calorimetry by taking into account muon energy loss in the calorimeters.

(2) To learn how to correct the energy loss for total muon energy measurement.

Figure 9 shows the energy loss spectra for muons with different muon energies at different calorimetry thickness (in terms of λ). The spectra peaks correspond to

the dE/dx energy loss, and the tails mainly come from muon bremsstrahlung energy loss in the calorimeter. For high energy muons such energy loss is significant, which implies that we have to collect the muon energy loss in the calorimeter to improve total muon energy resolution.

We have studied the method to correct the muon energy loss for total muon energy measurements:

$$E^{\mu}_{total} = P_{\mu-chamber} + \Delta E$$

where $P_{\mu-chamber}$ is the muon momentum measured in the muon chambers out side of the calorimeters. ΔE is the muon energy loss in the calorimeters. From the studies we determined that if $\Delta E < 1.27 \times E_{peak}$, we used E_{peak} to correct for the muon energy loss; otherwise we used ΔE measured by the calorimeters assuming an energy resolution of $\Delta E/E = 50\%/\sqrt{E} + 2\%$.

Figure 10 shows $\Delta p^{\mu}/p^{\mu}$ distributions using the above mentioned method compared with using only the calorimetry measured ΔE to correct for the muon energy losses. It is clear that the method we used improves the muon energy resolution significantly.

4 Total Muon Rate Calculations

We have used ISAJET Monte Carlo program to generate events for various processes of pp reactions. The final state particles then pass through the GEM detector (baseline design) simulation by parametrizations from the results of the GEANT simulations. Figure 11 shows the calorimeter material thickness (in λ) versus rapidity, η, for muon energy loss and the punchthrough rate calculations.

The following procedure was used in our simulation to calculate the total muon rate:

- ISAJET generate events with selected physics processes. For this study we included TWOJET(6 quarks and gluon jets, with 140 GeV Top mass), W+JET, Z+JET, and DRELL-YAN processes. Table 3 shows the number of generated events for each process.

- For each prompt muon, we calculated the pass-through thickness of calorimetry material according to the incident angle. The energy loss is simulated by the energy loss spectrum obtained in GEANT simulation of muons that are closest in both momentum and incident angle. dE/dx energy loss is corrected according to the calorimetry thickness.

- For each charged pions and kaons, the following procedures were used to generate the punchthrough particles:

  1. We first check if the particle should yield punchthrough particles in the muon chambers. The probability is calculated according to the spectra in figures 2 and 3.
  2. If there are charged punchthroughs in the muon chambers, the charged multiplicity was generated according to the distribution extrapolated from the distributions in Fig. 4.
  3. The energies and angular spread of the punchthrough particles are calculated according to the spectra shown in Figures 5, 6, 7 and 8. If there are more than three particles, their energies were generated based on the spectrum of the third leading energy particle (Fig. 7).
  4. The difference of punchthrough rates between outer layer and inner layer of the muon chambers were taken care by the difference of the first few bins of the normalized momentum spectra of inner and outer layers.
  5. For π^- and $k^\pm$ we used the spectra for π^+ of the same energy and incident angle.

- The total muon rates are calculated by combining the spectra from each physics process weighted by the cross section.

Fig. 12 shows the total rates in the inner layer muon chambers as functions of muon transverse momentum, p_T, in different rapidity ranges. Spectra from different physics processes were plotted to show their relative contributions.

Fig. 13 shows the total rates versus the rapidity, η, with different muon p_T cut. Without p_T cut, punchthroughs dominate the total rate. However with $p_T > 10$ GeV, the prompt muons dominate.

Fig. 14 shows the rate/cm^2 as functions of θ, with different hadron calorimeter thicknesses in the barrel region. We have assumed that the barrel inner layer muon chambers located at a distance of 3.7 m from the beam line, and endcap inner layer located at z=5.5 m (the beam line is along the z coordinate). We found that in the barrel region, the muon rate is roughly constant at 0.3 Hz/cm^2 for 12λ absorber, and about factor of 3 higher in the case of 10λ. In the endcap region, 14λ is necessary, since the rate increase exponentially as the angle decreases.

As a summary, Table 4 lists the muon rates in the inner layer of the muon chambers at several θ angles, with different p_T cuts, and Table 5 lists the integrated muon rates in various η regions. Table 6 lists the multi-muon event rates with different muon p_T cuts.

5 Discussions and Conclusions

5.1 Rate Calculation Uncertainties

Muon chamber and trigger design need to know the total muon rates. It is important to understand the calculation uncertainties for the designs. We list the calculation uncertainty contributions in the following:

- **GEANT simulation energy cut off:** we set the shower development energy

cut off at 0.1, 0.5 and 1.0 GeV for muons, hadrons and electron/photon respectively to speed up the simulations (if the GEANT default energy cutoff values were used, at least 5 times more CUP hours would be needed). In order to check our calculation uncertanties, we have used the GEANT default energy cutoff values (see Table 2) to study the punchthrough probabilities with 10 GeV and 20 GeV pions at different angles. We compared the punchthrough probabilities from low cutoff runs with our standard cutoff runs, and found that the differences were at 30% level. We therefore estimated our punchthrough probability calculations with an uncertainty of $\sim$ 30% for energy less then 0.5 GeV charged particles. It is clear that this uncertainty will not affect the muon trigger rates if we consider triggering on muons with p_T >5 GeV. However muon inner chamber hit occupancy should be higher than what we have presented.

- **Extrapolation of punchthrought spectra:** We have used momentum spectra obtained from pions at certain incident angles. Particles with incident angles different from these values can have different flight decay probabilities. We also used only spectra of 50, 100, 200, and 500 GeV pions. The punchthrough spectra of low energy pions (<20 GeV) show significantly increase of flight decays, which are not in the 50 GeV spectrum. We estimated that these effects can cause an rate uncertainty of $\sim$ 10%.

- **Theoretic model:** quark hadronization, which determines charged multiplicity of jets, in ISAJET program was tuned by UA1 data, extrapolation to the SSC energy scale gives uncertainties. It is not clear to us how much does this contribute to the rate uncertainties.

- **Small angle detector geometry:** for $|\eta|$> 2.5, the rate calculation using parametrization method has large uncertainty since hadronic showers spread into the detector hole around the beam. Also charged particles interacting with the beam pipe in the small angle will knock out many showered particles and increase the occupancy of the small angle muon chambers. Therefore, without detail detector and beam pipe shielding design and using full GEANT

simulation, the calculation is not reliable. In this study, we used only the calculation results above 9° .

- **Cosmic rays and beam spread :** The calculation reported in this paper doesn't include the contributions from cosmic rays and beam spread.

In summary, considering the above uncertainties in our calculations the real occupancy rate in the muon chamber will be higher than our results. A safety factor of ~3 should be used for chamber and trigger designs based on these results.

5.2 Applications of the Results

- *Muon Level-1 Trigger*

The GEM collaboration proposed to use Resistive Plate Counters "RPC's", which have a response time of less than 10 nanoseconds, and Cathod Strip Chamber "CSC's", which have a response time of less than 15 nanoseconds (wire spacing for "CRC's" is 2.5 mm), as the fast muon trigger devices for the barrel and the endcap regions respectively. The "RPC's" can handle a rate of 40 Hz/cm^2, which is limited by chamber dead time. The "CSC's" in principle can handle a rate up to 100 kHz/stripe, which is limited by signal integration time. Figure 14 shows that even at $10^{34}/cm^2/s$ luminosity, the total muon rate in the barrel region is about 3 Hz/cm^2, "RPC's" certainly can hadle this rate with large safety factor. In the endcap regions, the total muon rate in inner muon chambers can be as high as 200 Hz/cm^2 at the $10^{34}/cm^2/s$, the "CSC's" can be easily designed to work on such rate.

Fast muon trigger is generated from roads in three layers of "RPC's" or "CSC's". Roads are formed by few centimeter wide strips in the central "RPC's", and by radial cathod strips and vertical wires in the endcaps. According to Table 5, the total muon rate ($|\eta| < 2.5$) with $p_T^\mu > 5$ GeV is about 10 kHz, and with $p_T^\mu > 25$ GeV is about 1 kHz at the SSC standard luminosity. If the Level-1 trigger is designed to handle a few tens of kHz, then it is possible to trigger on muons with 5 GeV p_T threshold at

$10^{33}/cm^2/s$ luminosity, and with 25 GeV p_T threshold at $10^{34}/cm^2/s$.

- *Muon Chamber Occupancy*

Assuming that the barrel muon chambers are made of 4 meters long drift tubes with 4 cm diameters. Based on Fig. 14, the rate per tube would be about 500 Hz at the SSC standard luminosity. The occupancy can be estimated as $rate \times T_{max}$, where T_{max} is the maximum drift time of the tube. Assuming $T_{max} = 1\mu s$, the occupancy would be about 5×10^{-4} at $10^{33}/cm^2/s$ luminosity, and 5×10^{-3} when the luminosity increases by a factor of 10.

If the endcap muon chambers are made of "CSC's" (also called PAD chambers) with 0.5 cm wide and 1 meter long cathod strips. The occupency would be less than 0.1% at the standard luminosity. Here we assumed the strip integration time to be 1 μs, and that one charged particle signals three pads. From this result we believe that it will also work at higher luminosities.

5.3 Conclusions

We conclude, based on our simulations, that:

- At the high luminosity hadron colliders, muons certainly offer an advantage over electrons/photons due to the low particle rate outside of the calorimeter. We can trigger on muons with the p_T cut as low as 5 GeV. Such low p_T cut is very important for increasing the event acceptance in events like $H^0 \rightarrow ZZ^* \rightarrow \mu\mu\mu\mu$.
- Muon chamber located outside the calorimeter can certainly work at the $10^{34}/cm^2/s$ luminosity.
- Except from the uncertainties in the theoretical models, this simulation should be accurate to within a factor of 2 for $|\eta| < 2.5$. For small angle $|\eta| > 2.5$ muon chamber and trigger design, one needs full GEANT simulation with completely

defined detector geometry.

Acknowledgement

We would like to thank the Texas National Research Laboratory Commission for their support through the SSC fellowship program, and providing essential computer equipements for this study. We thank the Laboratory for Nuclear Science of MIT and the SSC lab. for supporting our calculations.

References:

[1] R. Brun et al., GEANT (version 3.14) CERN DD/EE/89-1, Sept. 1990;

[2] F. Paige and S. D. Protopopescu, ISAJET (v. 6.36) A Monte Carlo Event Generator for PP and $\bar{P}P$ reactions, July, 1991.

[3] H. Fesefeldt, GHEISHA, RWTH Aachen preprint PITHA 85/02 (1985).

Figure Captions

Figure 1 Side view of detector geometry set up for GEANT Monte Carlo simulations.

Figure 2 Singel π^+ punchthrough probabilities as functions of energy of the incident π^+ and the absorber thickness.

Figure 3 Comparison of the punchthrough probabilities of π^+, π^-, k^+, and k^-.

Figure 4 In total 12 figures show the single pion punchthrough charged multiplicity distributions at different pion energy and absorption length. Shaded histograms show the muon component in the punchthrough particles.

Figure 5 In total 12 figures show the normalized momentum spectrum of the leading energy punchthrough particle. Open histogram corresponds to the inner chamber spectrum, and shaded histogram corresponds to the outer chamber spectrum. The difference is due to the low energy particle looping inside the magnetic field.

Figure 6 In total 12 figures show the normalized momentum spectrum of the second leading energy punchthrough particle. Open histogram corresponds to the inner chamber spectrum, and shaded histogram corresponds to the outer chamber spectrum. The difference is due to the low energy particle looping inside the magnetic field.

Figure 7 In total 12 figures show the normalized momentum spectrum of the third leading energy punchthrough particle. Open histogram corresponds to the inner chamber spectrum, and shaded histogram corresponds to the outer chamber spectrum. The difference is due to the low energy particle looping inside the magnetic field.

Figure 8 In total 12 figures show the punchthrough particle angular spread correlated to the normalized momentum.

Figure 9 In total 12 figures show the muon energy loss distributions for differnt muon energies and absorber thicknesses.

Figure 10 Muon energy resolution distributions for 20 GeV and 50 GeV muons. Solid histograms were obtained using the method described in section 3.2. Dashed histograms were obtained by adding energy loss measured in the calorimeters only.

Figure 11 Calorimeter interaction length as a function of the rapidity used in our total rate calculations.

Figure 12 Total muon rates versus muon transverse momentum (p_T). Contributions from different physics processes are also shown. (a) $|\eta| < 1.5$, (b) $1.5 < |\eta| < 2.0$, (c) $2.0 < |\eta| < 2.5$, (d) total rate with $|\eta| < 2.5$.

Figure 13 (a) Total muon rates as functions of the rapidity with different muon p_T cuts. (b)-(f) show the total muon rates as well as contributions from different physics processes, with different muon p_T cuts. Note that the rates at the positive and negative rapidity have been folded together in this figure.

Figure 14 Inner muon chamber hits rate per cm^2 versus the polar angle, θ. For this figure we assumed that the inner barrel chambers are located at 3.7 meters from the beam line in the case of 12λ, and 3.5 meters in the case of 10λ. The inner endcap chambers were assumed to be located at 5.5 meters from the interaction point.

Table 2: **List of Number of Single Hadron Simulated**

cutoff energy: 0.1, 0.5, 1.0 GeV for μ, hadron and γ/e respectively								
P (GeV)	10	20	50	100	200	300	400	500
θ=90° (λ=11.8)	250k	200k	620k	115k	126k	64k	53k	110k
θ=15° (λ=14.5)	1070k	4k	2385k	782k	113k	100k	100k	164k
θ=25° (λ=15.5)	100k	13k	2132k	100k	50k	50k	10k	10k
θ=45° (λ=17.0)	89k	16k	1194k	23k	10k	10k		
θ=70° (λ=12.8)	100k	100k	100k	100k	100k	100k	100k	
θ=90° (λ=10)	1100k	100k	100k	100k	80k		40k	40k
cutoff energy: 0.01, 0.01, 0.001 GeV for μ, hadron and γ/e respectively								
θ=90° (λ=11.8)	100k	50k						
θ=15° (λ=14.5)	100k	50k						
θ=25° (λ=15.5)	100k	50k						
θ=45° (λ=17.0)	100k	50k						
θ=70° (λ=12.8)	100k	50k						

Table 3: **Simulated MC Events in Various Physics Processes**

process	P_T^{jet}(GeV)	cross section(mb)	N_{MC}
Minimal bias	4-20	7.4×10^{1}	1000k
$PP \rightarrow 2$ jets (q, g)	20-9000	0.2×10^{1}	9700k
$PP \rightarrow t\bar{t}$	10-5000	1.6×10^{-5}	1150k
$PP \rightarrow W + X \rightarrow \mu\nu X$	10-5000	3.1×10^{-5}	1770k
$PP \rightarrow Z + X \rightarrow \mu^+\mu^- X$	10-5000	3.1×10^{-6}	800k
$PP \rightarrow \gamma(Z) + X \rightarrow \mu^+\mu^- X$	10-5000	5.1×10^{-6}	432k

Table 4: **Particle Rate (Hz/degree) at Several Angles**

Angle	90°	70°	45°	25°	15°
no p_T cut	2.4k	3.0k	10k	23k	45k
$p_T > 5$ GeV	13	24	45	70	140
$p_T > 10$ GeV	4	5	8	20	30
$p_T > 15$ GeV	1.5	2.2	3.3	4.5	7
$p_T > 20$ GeV	0.8	1.1	1.5	2.0	3.0

Table 5: **Integrated Rate (Hz) in Several η Regions**

Region	$\mid \eta \mid < 2.5$	$\mid \eta \mid < 1.5$	$1.5 < \mid \eta \mid < 2$	$2 < \mid \eta \mid < 2.5$	di-muon $\mid \eta \mid < 2.5$
no p_T cut	2467k	1042k	660k	760k	230k
$p_T > 5$ GeV	9.31k	1.84k	2.23k	2.23	91
$p_T > 10$ GeV	1.92k	1.08k	440	403	19
$p_T > 15$ GeV	630	372	136	120	9.9
$p_T > 20$ GeV	280	166	52	58	6.3
$p_T > 25$ GeV	140	50	26	24	

Table 6: **Multi-Muon Event Rate (Hz) for $\mid \eta \mid < 2.5$**

multi-μ state	1μ/event	2μ/event	3μ/event	4μ/event	$> 4\mu$/event
no p_T cut	1274k	144.7k	42.7k	19.3k	24.1k
$p_T > 5$ GeV	9.14k	88	1.84	0.17	0.022
$p_T > 10$ GeV	1.91k	17.4	0.52	0.14	0.016
$p_T > 15$ GeV	629	8.36	0.30	0.12	0.014
$p_T > 20$ GeV	280	4.95	0.20	0.092	0.013

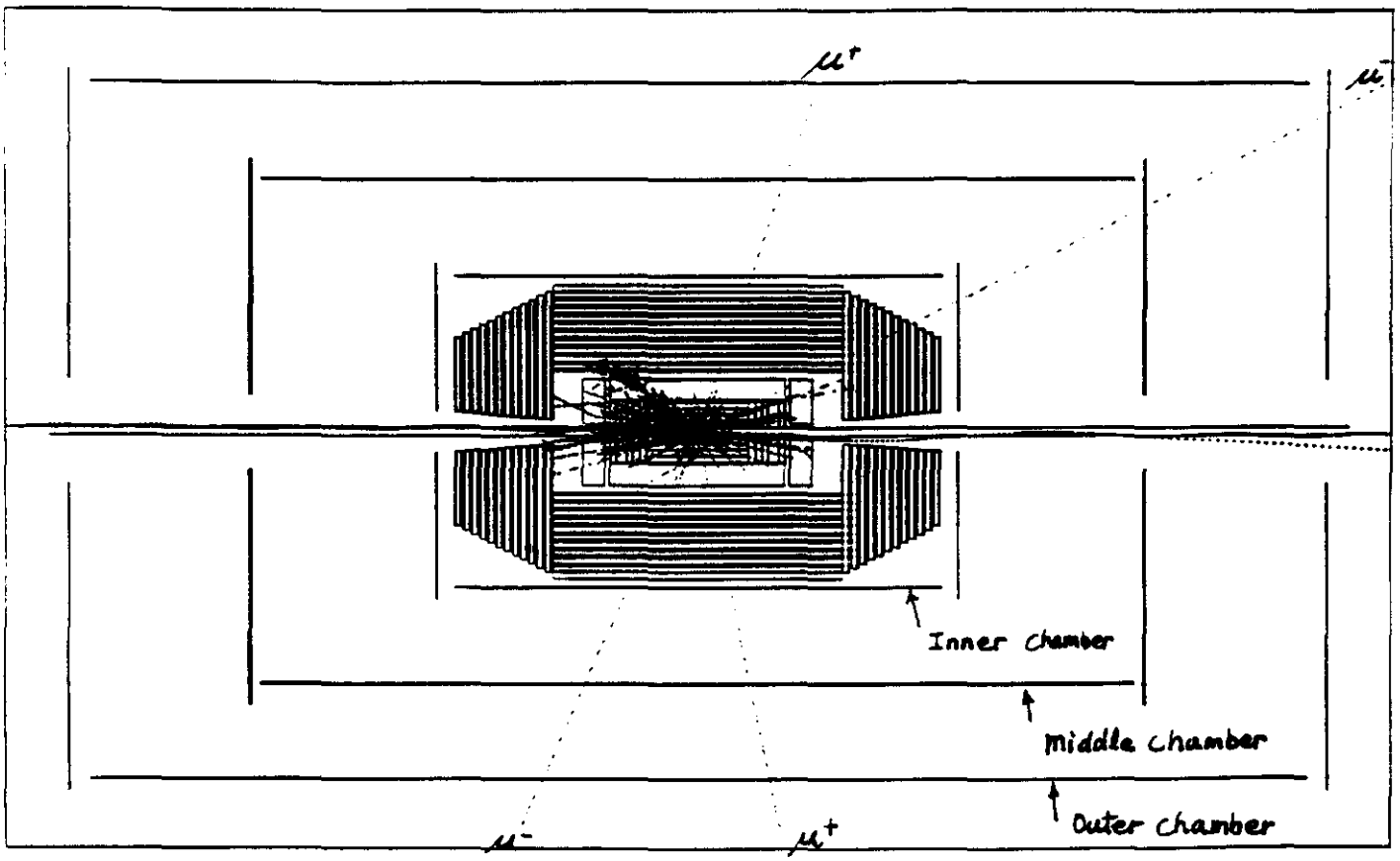

Figure 1 Side view of detector geometry set up for GEANT Monte Carlo simulations.

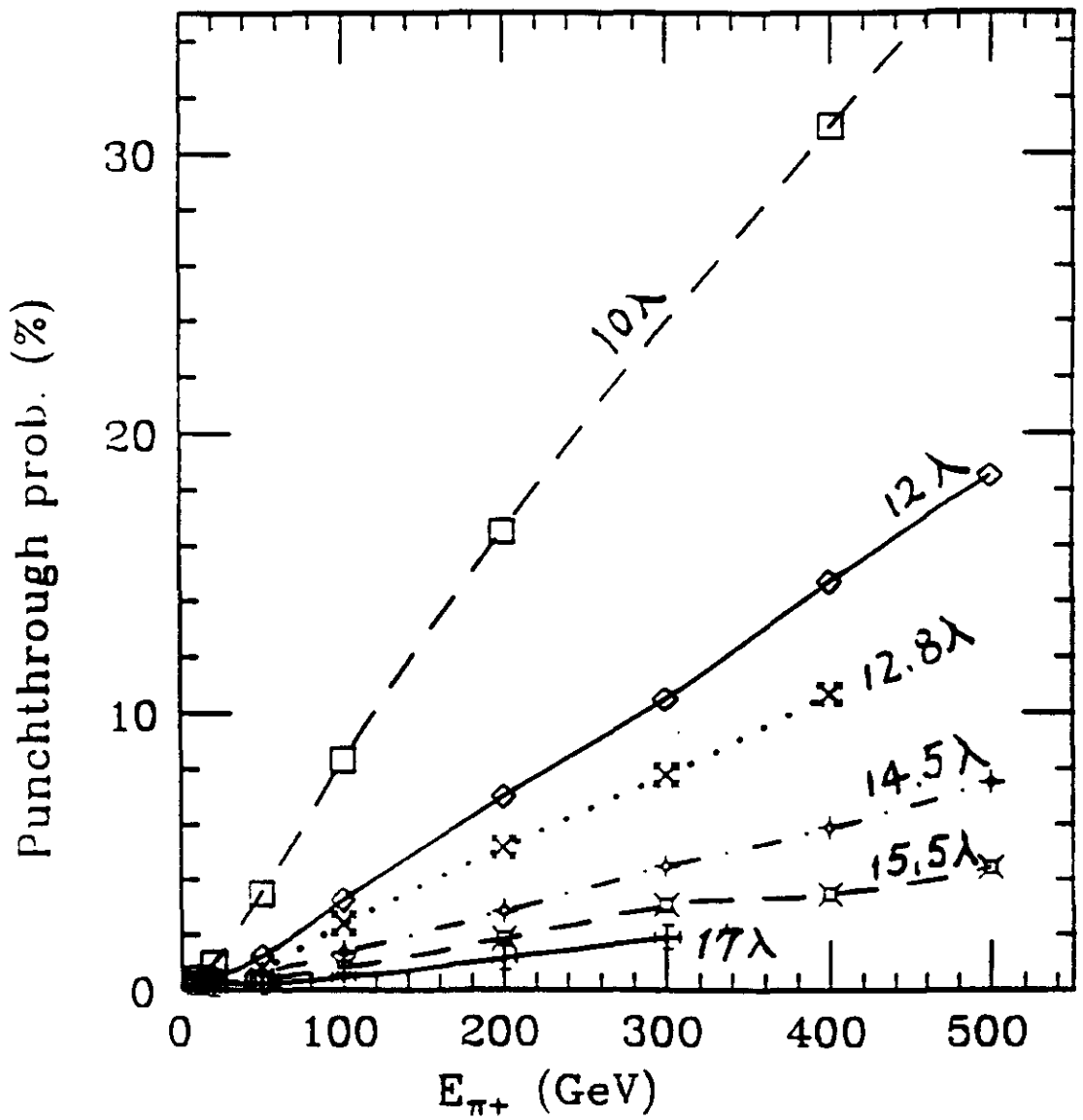

Figure 2 Singel π^+ punchthrough probabilities as functions of energy of the incident π^+ and the absorber thickness.

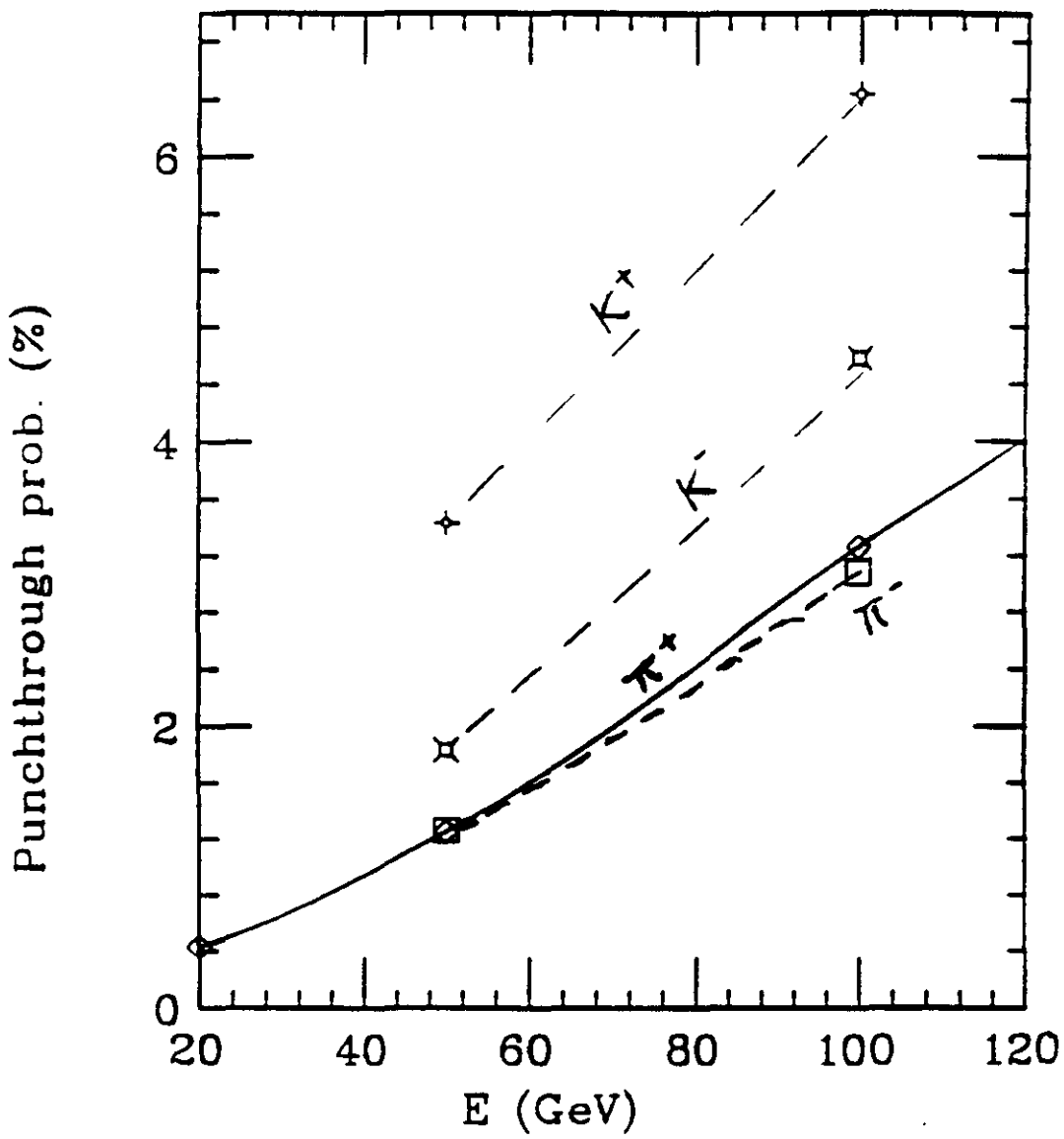

Figure 3 Comparison of the punchthrough probabilities of π^+, π^-, k^+, and k^-.

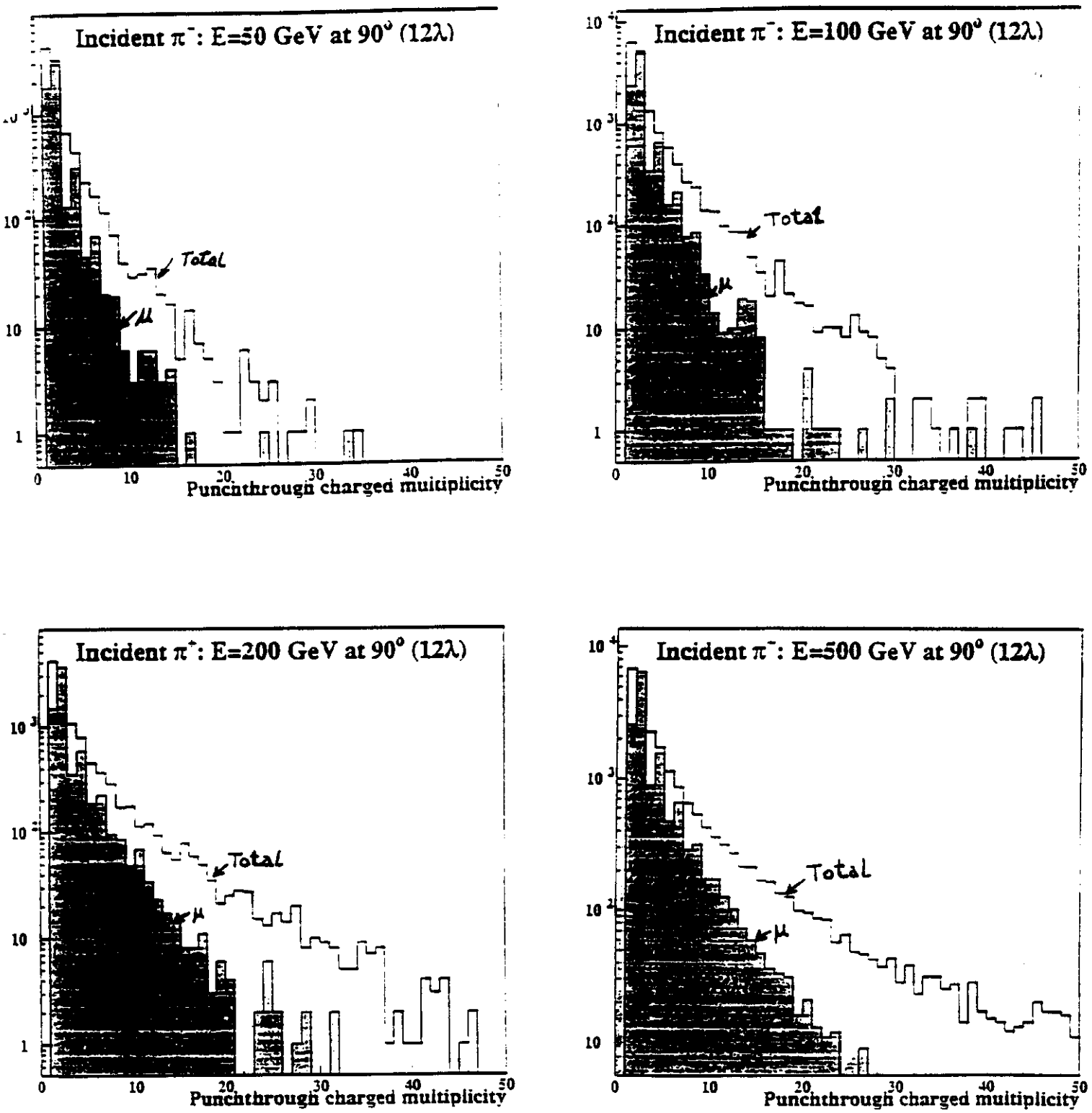

Figure 4 In total 12 figures show the single pion punchthrough charged multiplicity distributions at different pion energy and absorption length. Shaded histograms show the muon component in the punchthrough particles.

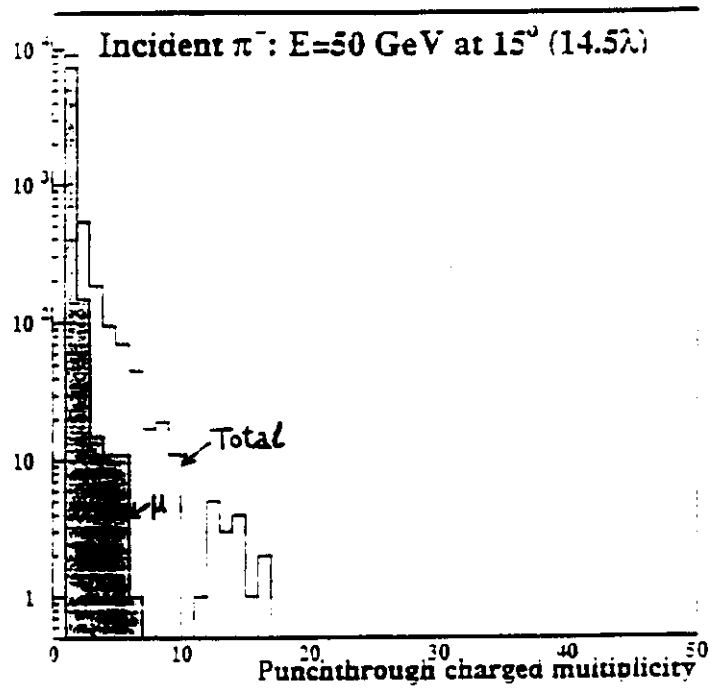

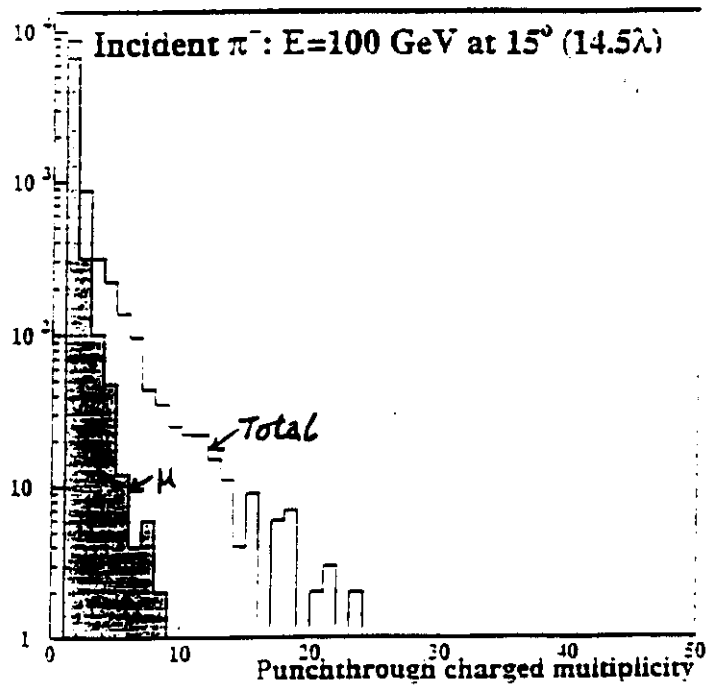

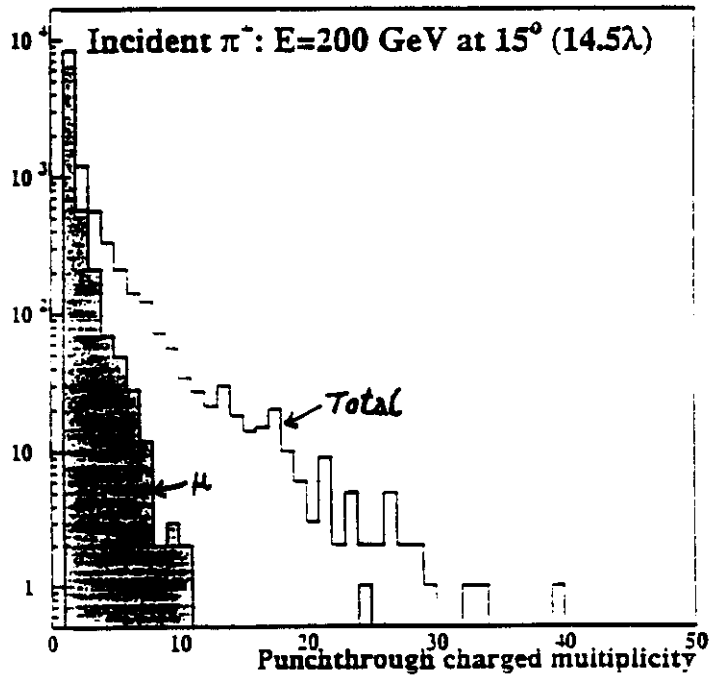

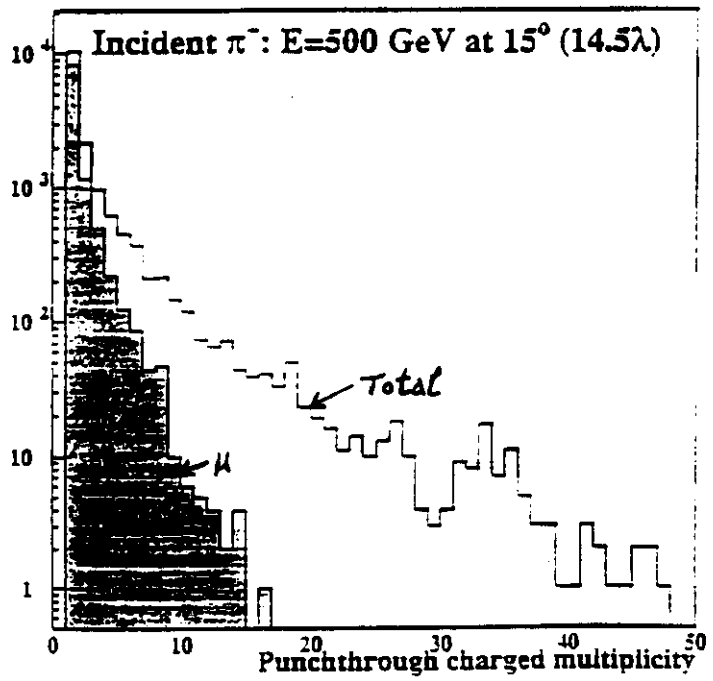

Fig. 4 Contine

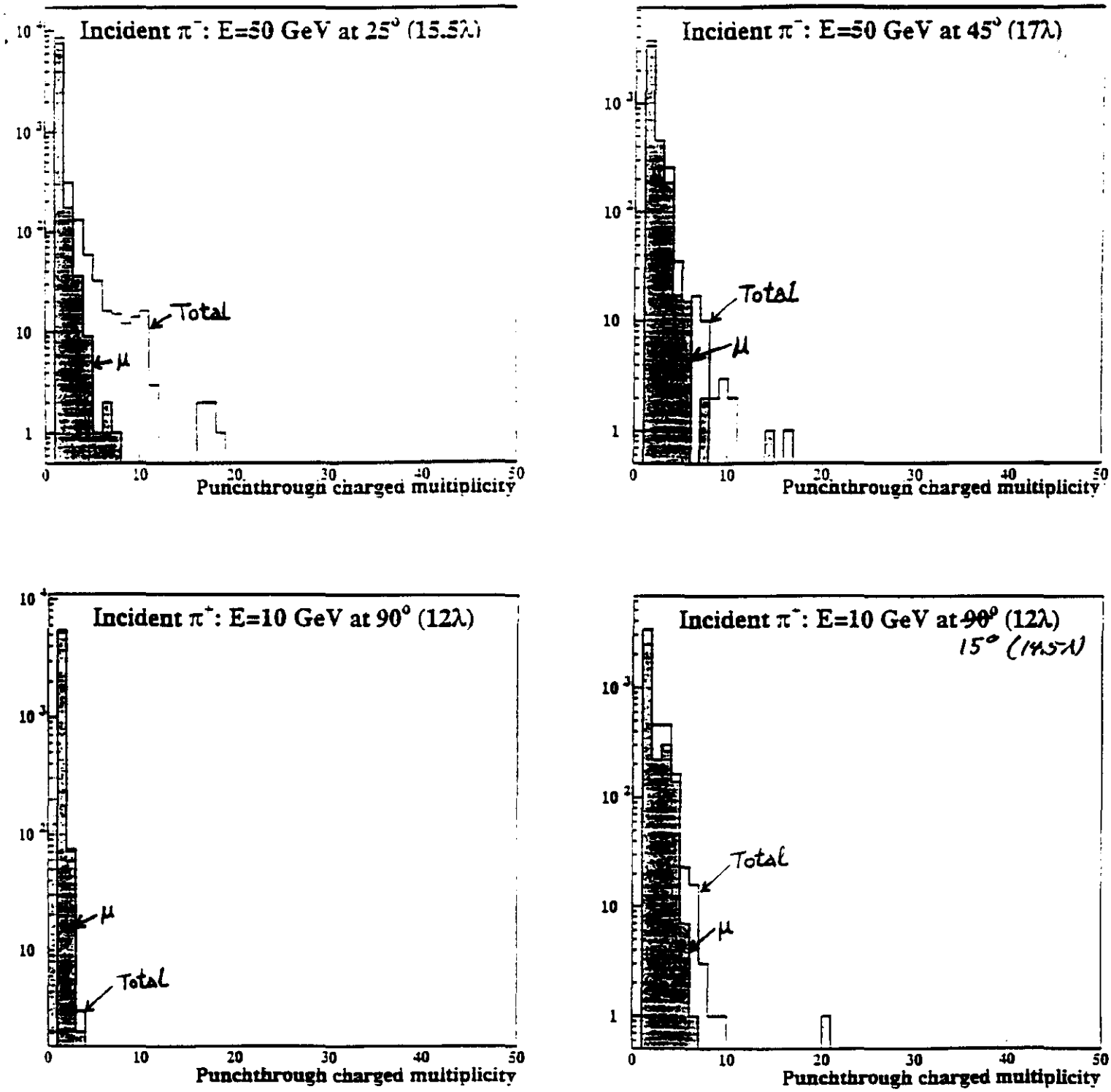

Fig. 4 Continue

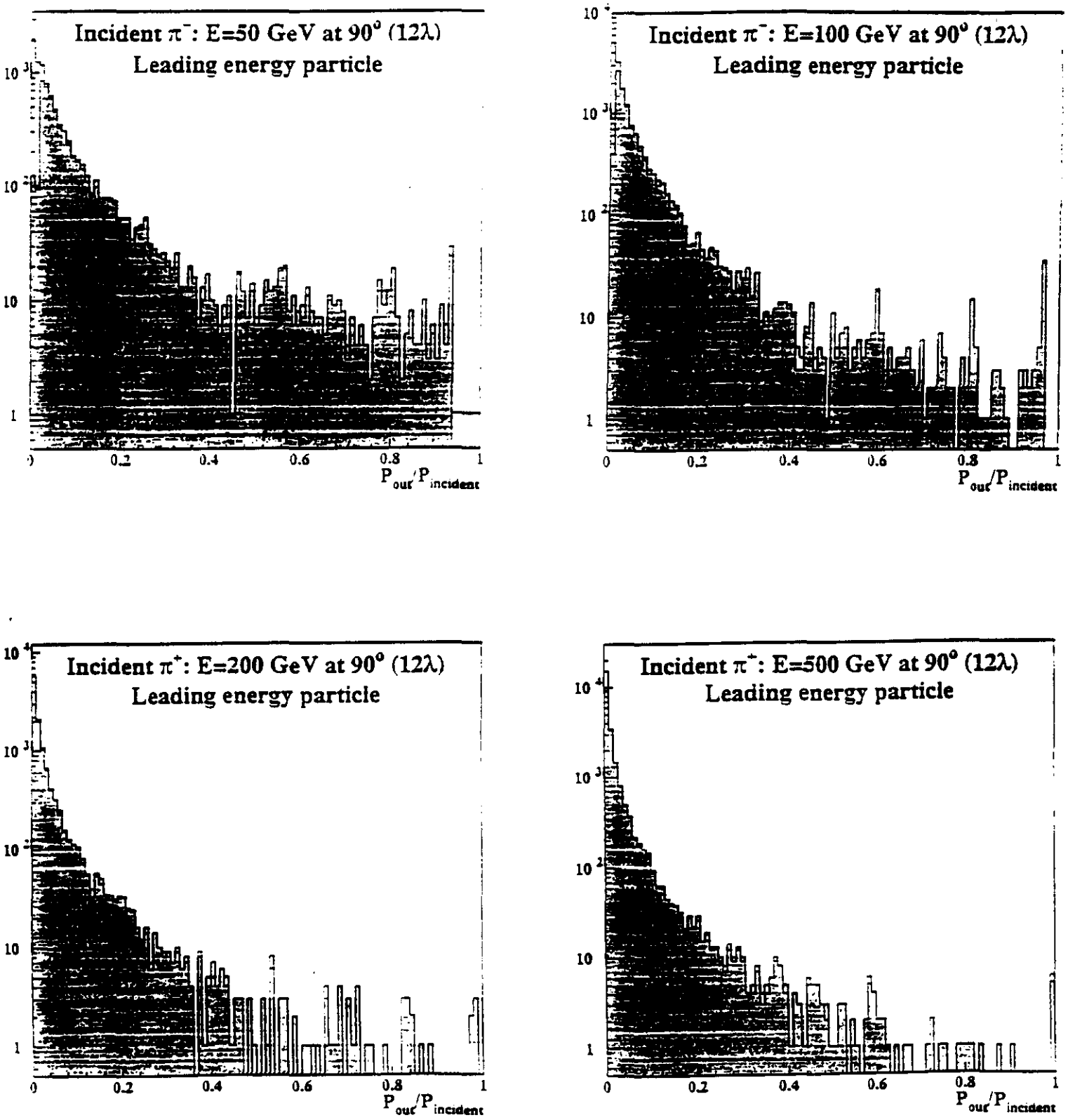

Figure 5 In total 12 figures show the normalized momentum spectrum of the leading energy punchthrough particle. Open histogram corresponds to the inner chamber spectrum. and shaded histogram corresponds to the outer chamber spectrum. The difference is due to the low energy particle looping inside the magnetic field.

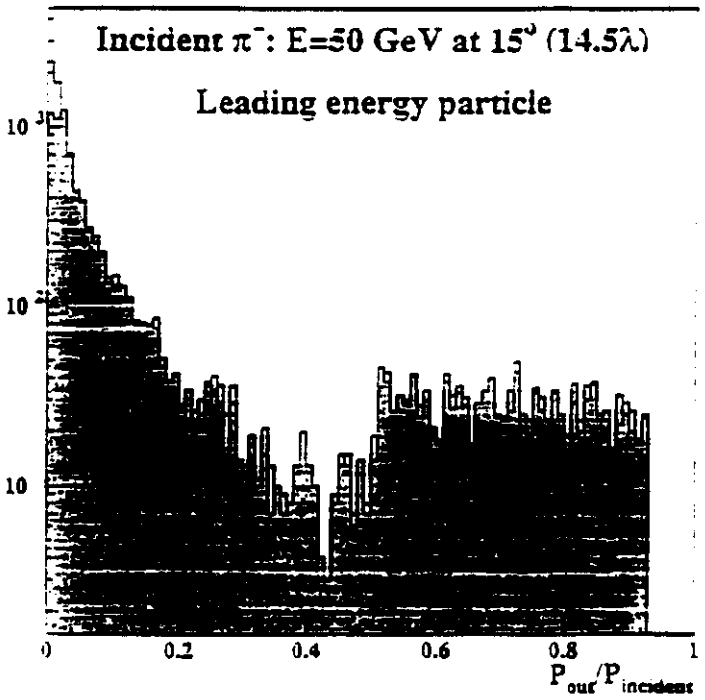

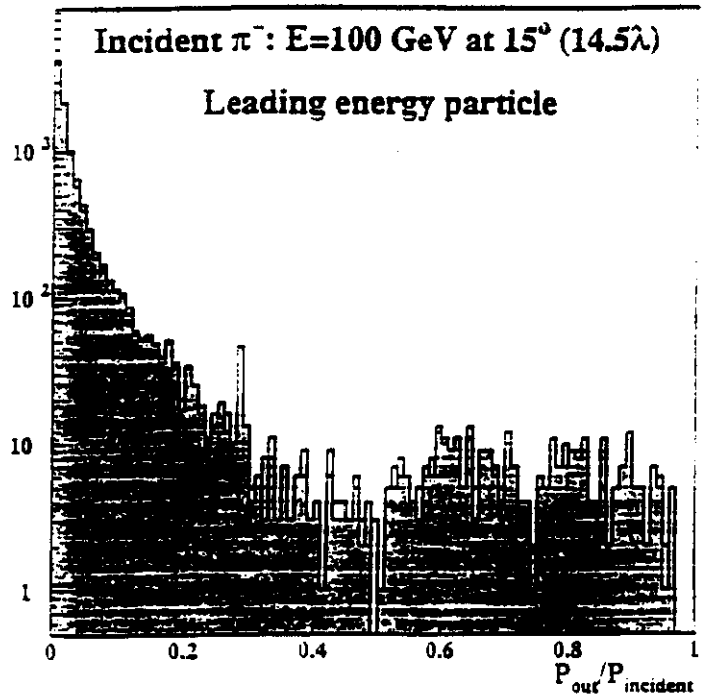

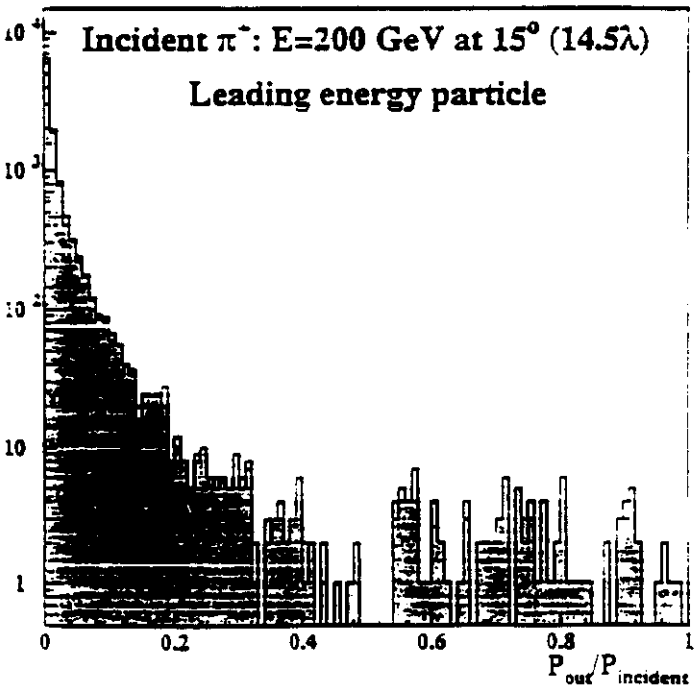

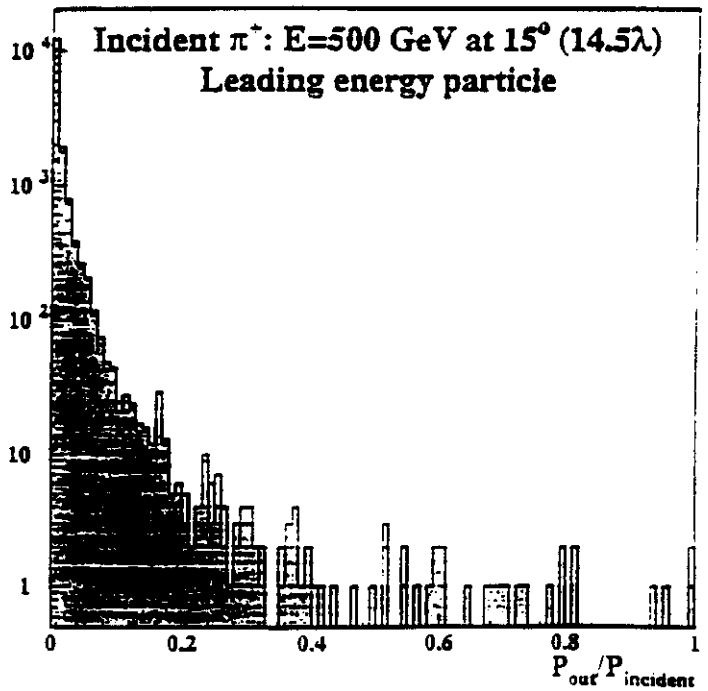

Fig. 5 Continue

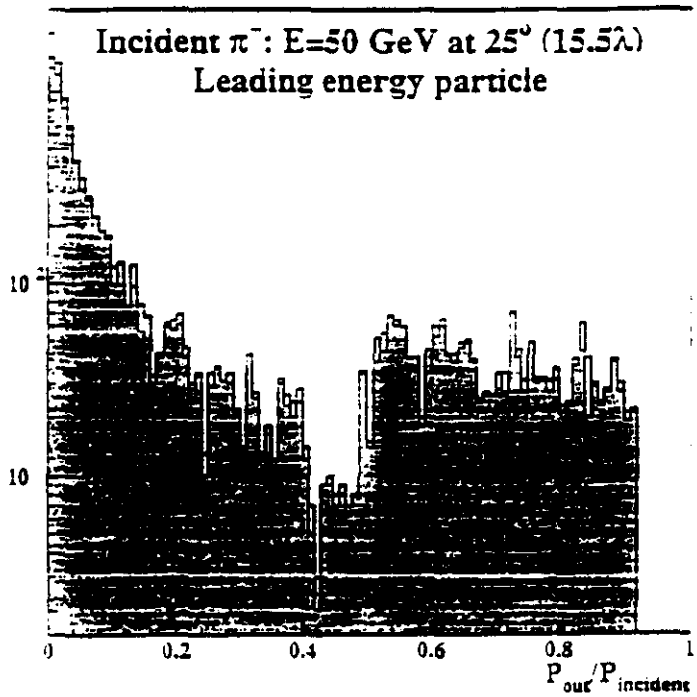

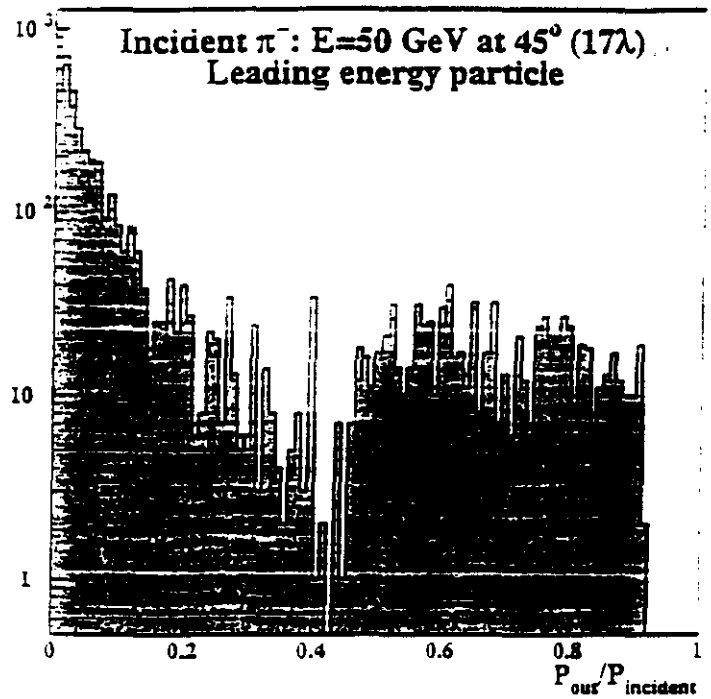

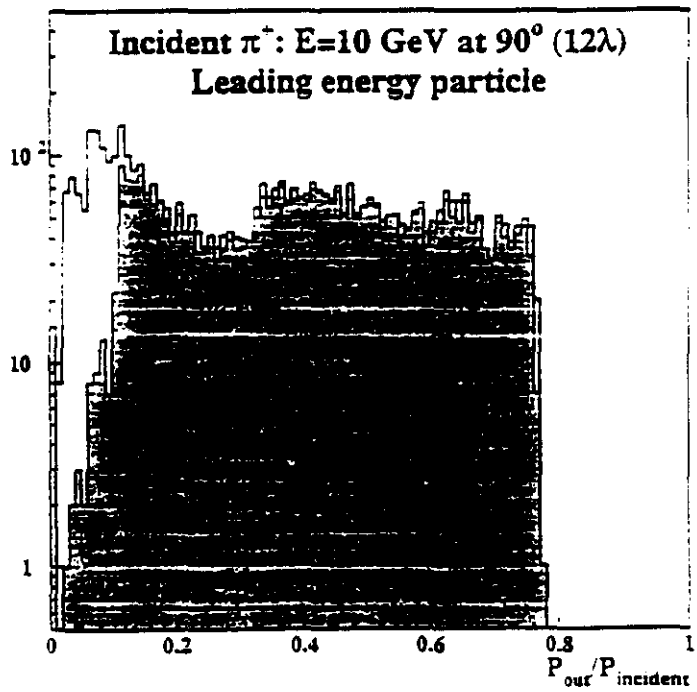

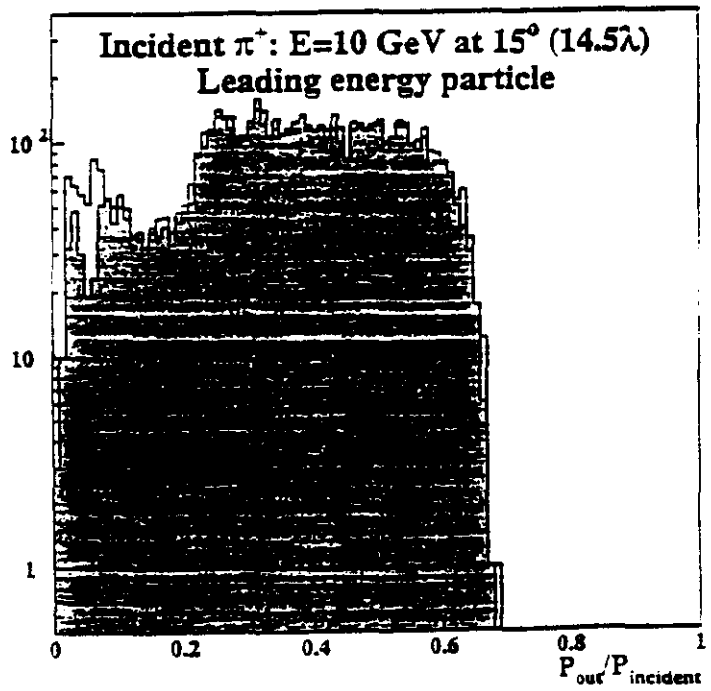

Fig. 5 Continue

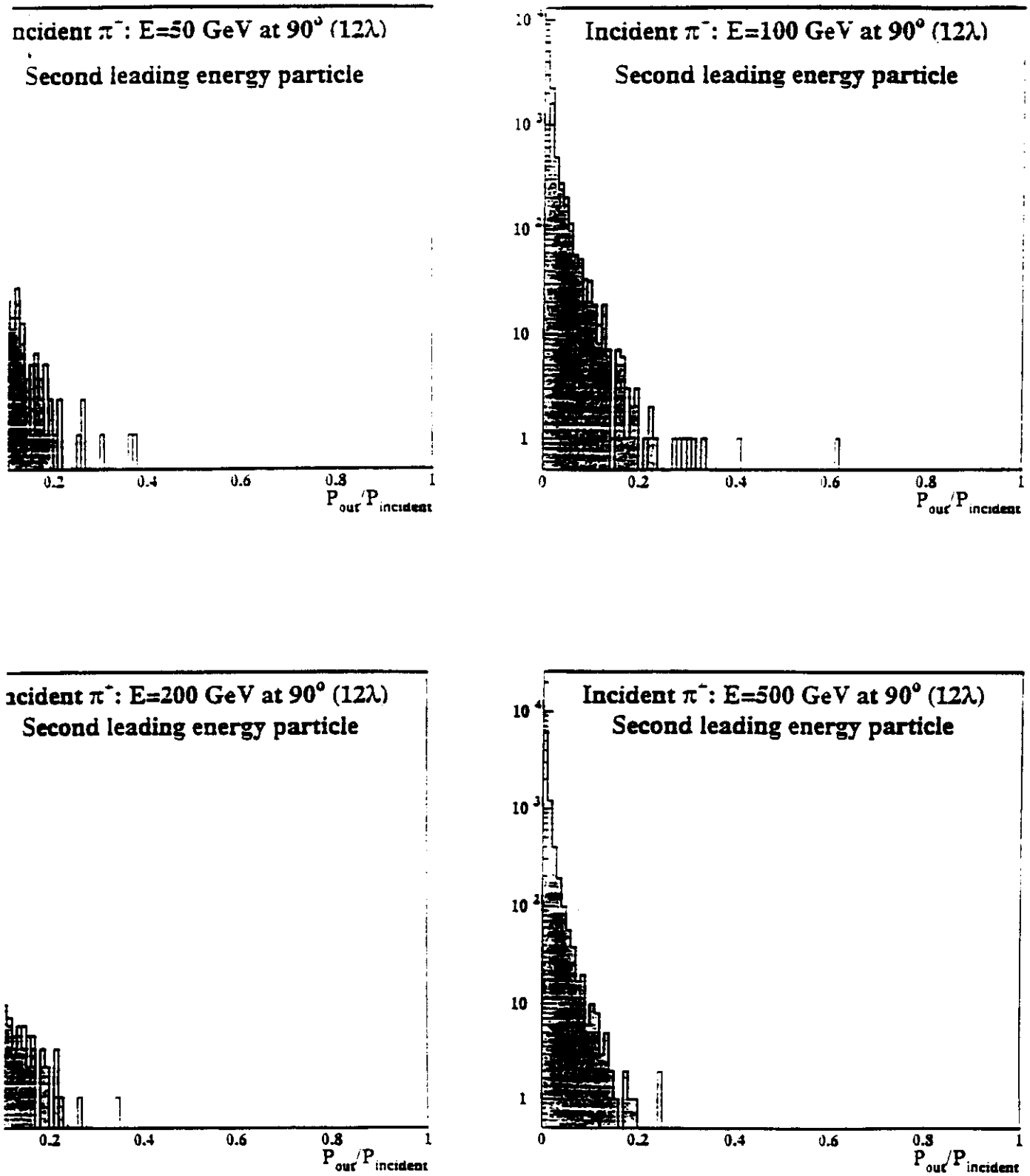

Figure 6 In total 12 figures show the normalized momentum spectrum of the second leading energy punchthrough particle. Open histogram corresponds to the inner chamber spectrum, and shaded histogram corresponds to the outer chamber spectrum. The difference is due to the low energy particle looping inside the magnetic field.

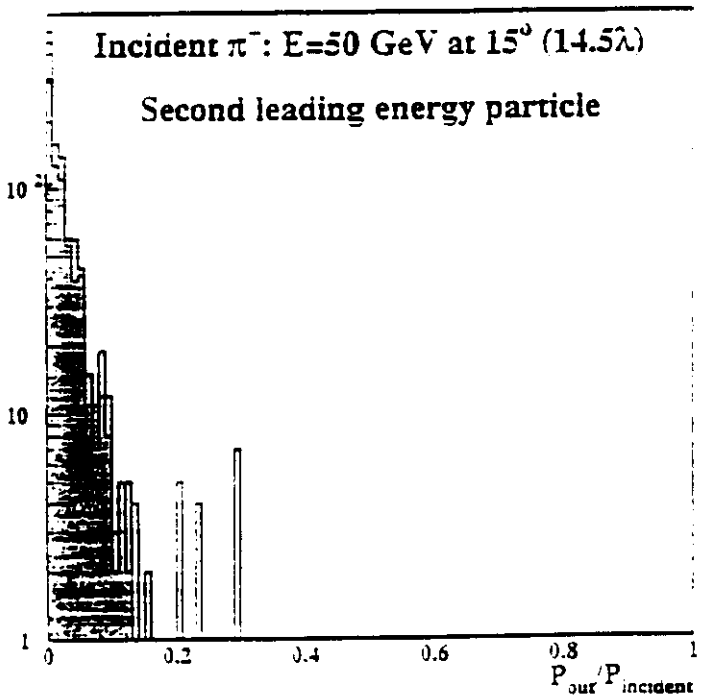

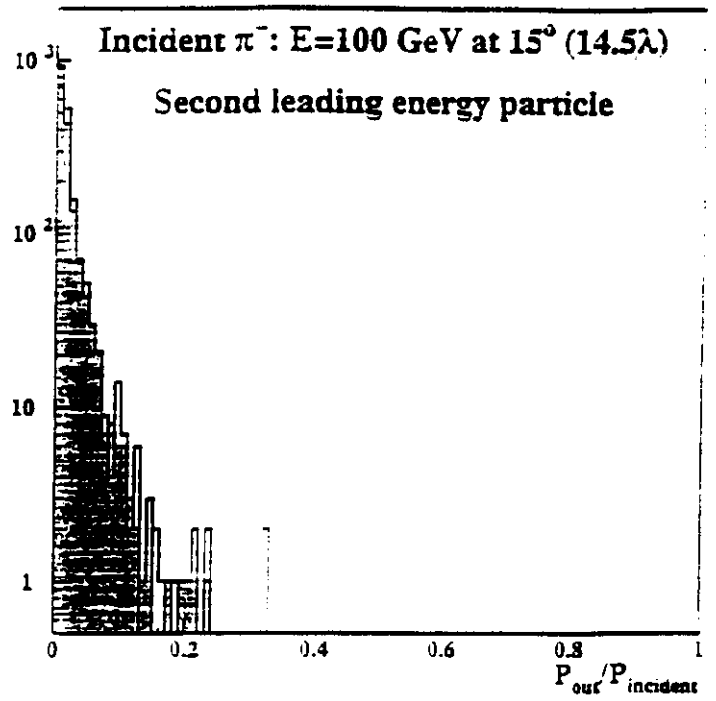

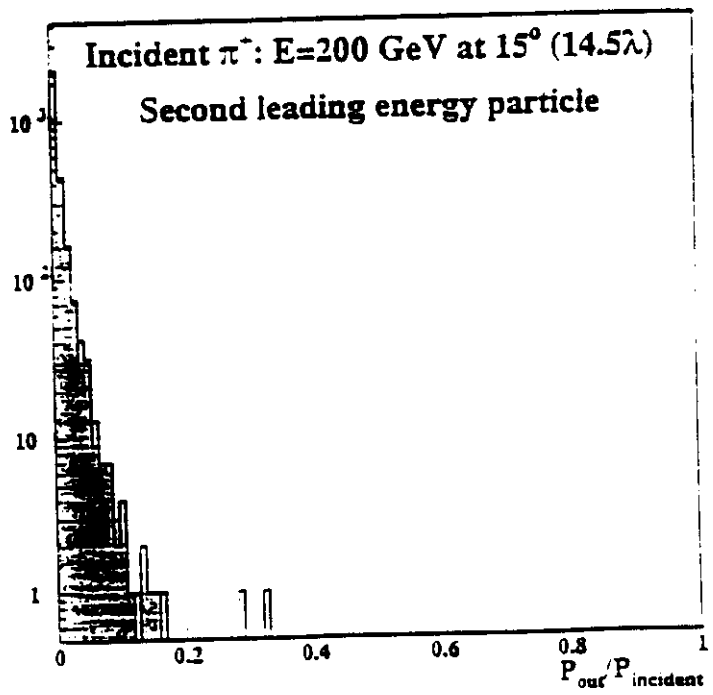

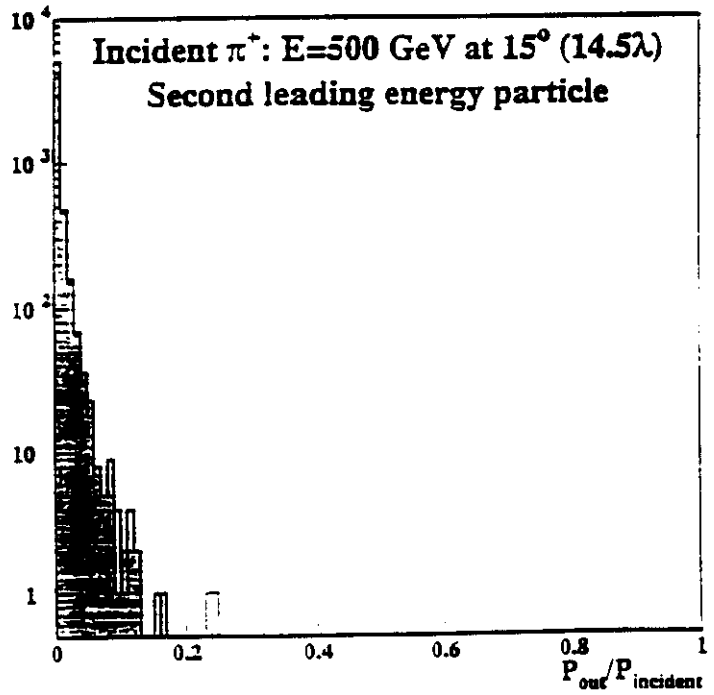

Fig. 6 continue

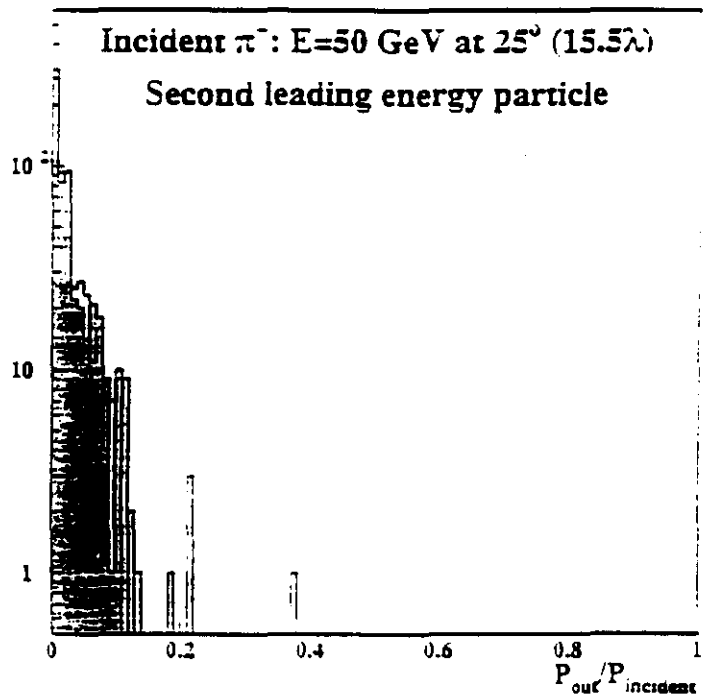

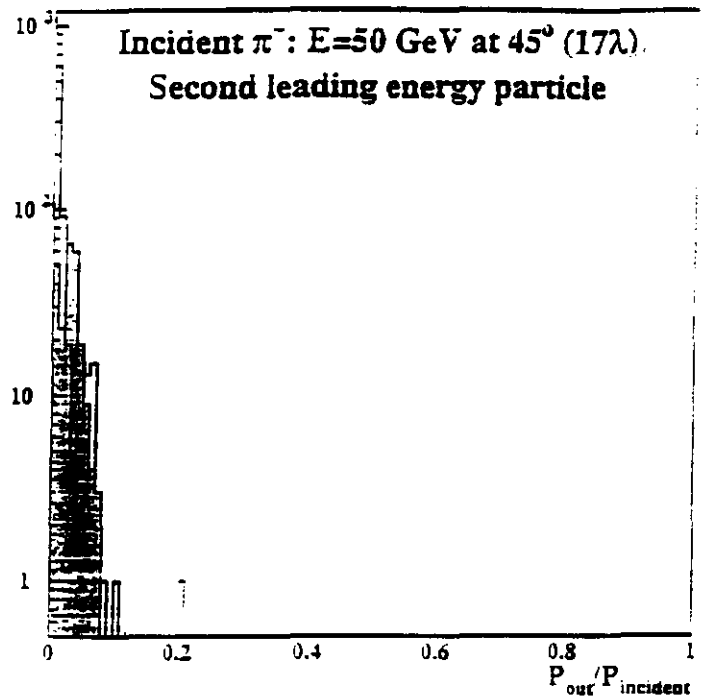

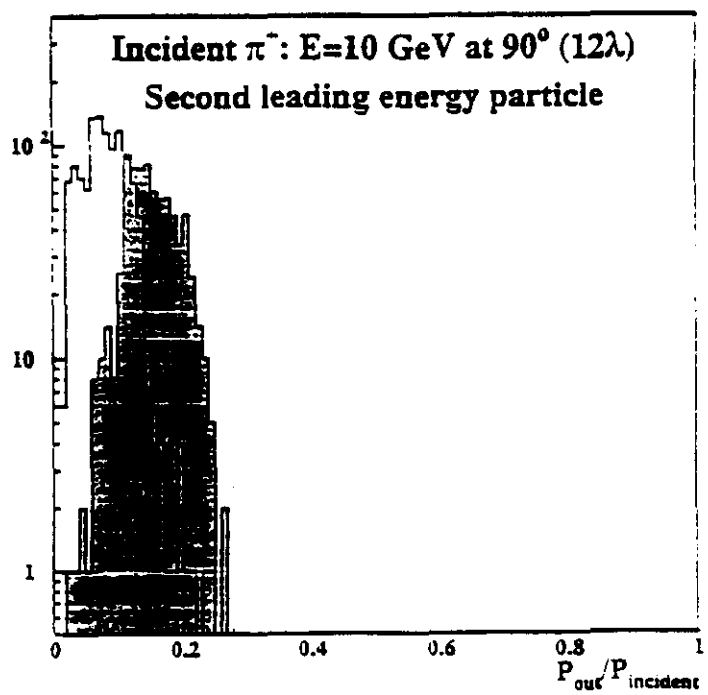

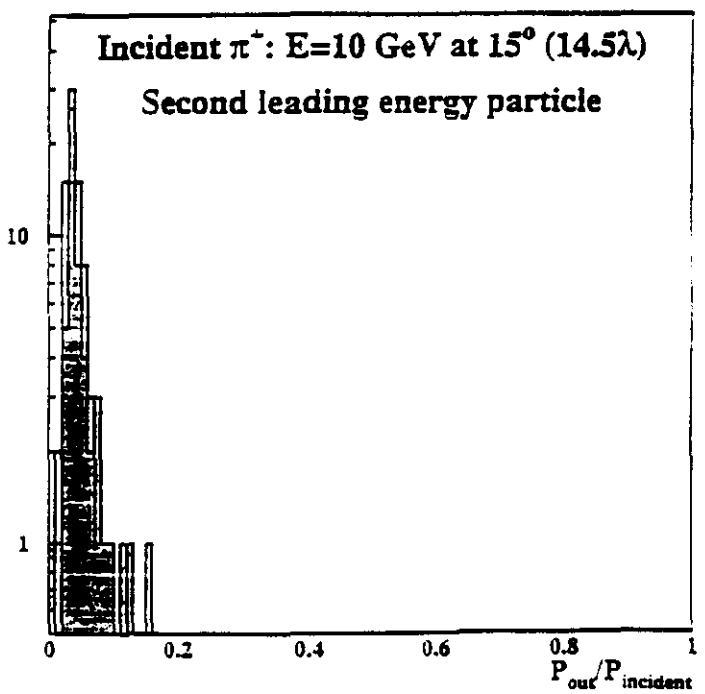

Fig. 6 continue

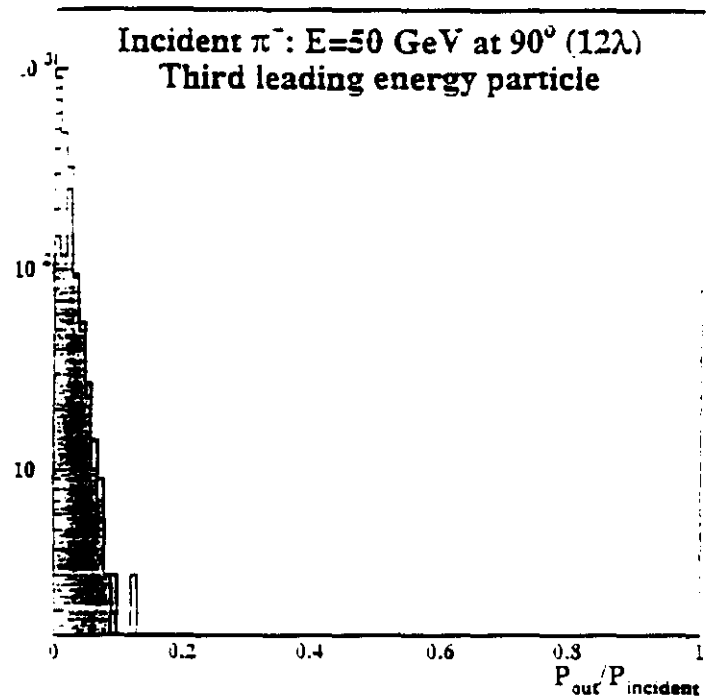

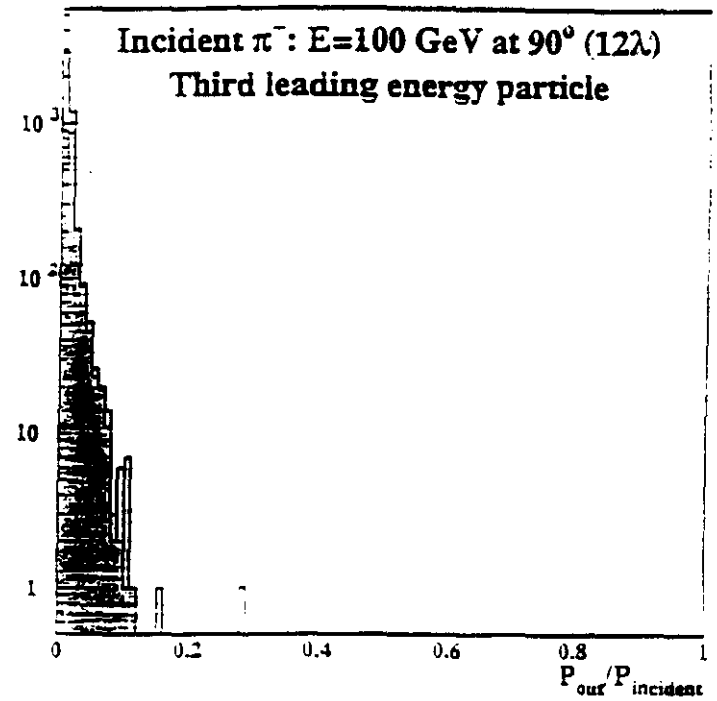

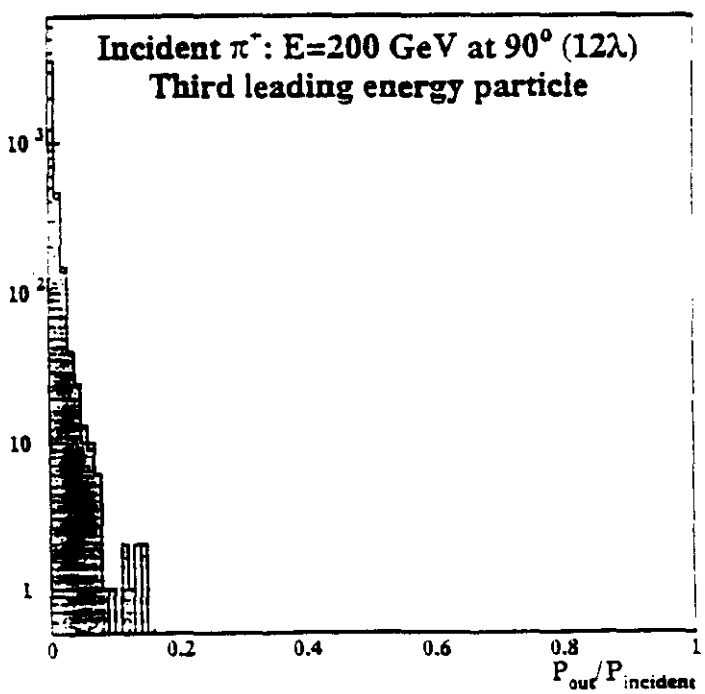

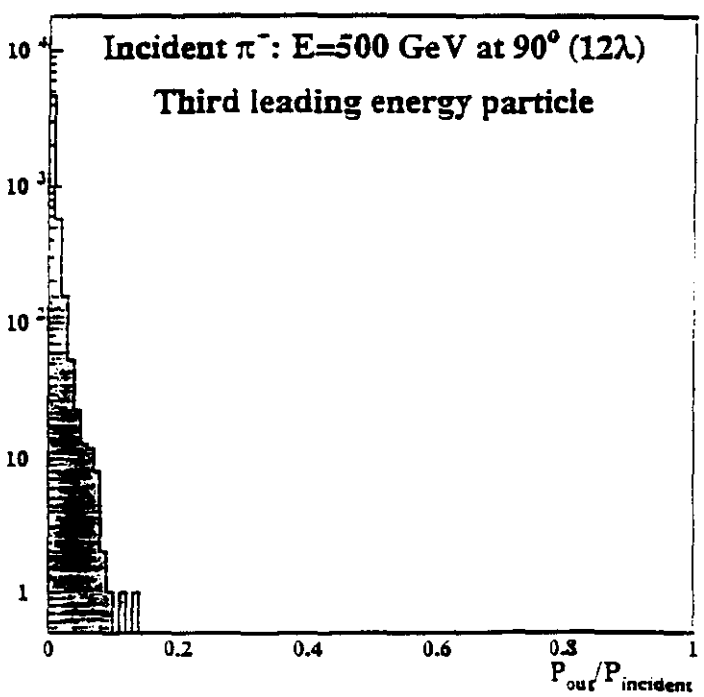

Figure 7 In total 12 figures show the normalized momentum spectrum of the third leading energy punchthrough particle. Open histogram corresponds to the inner chamber spectrum, and shaded histogram corresponds to the outer chamber spectrum. The difference is due to the low energy particle looping inside the magnetic field.

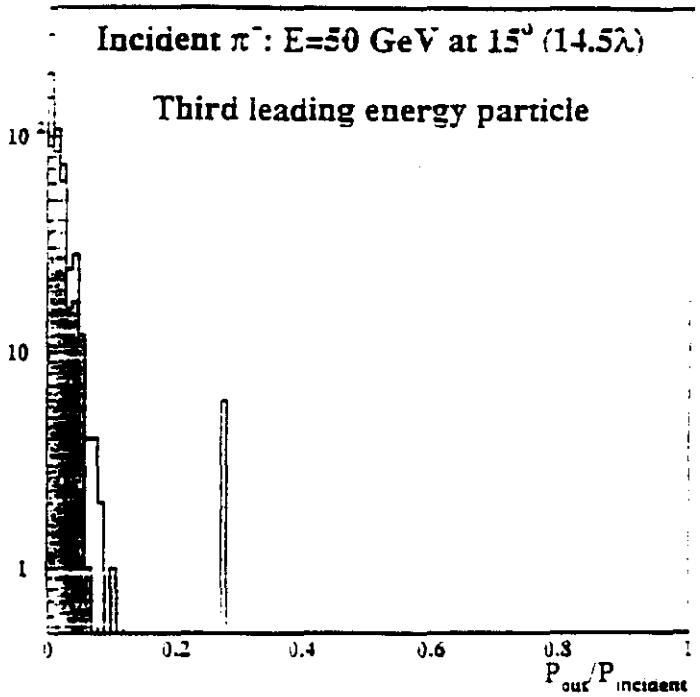

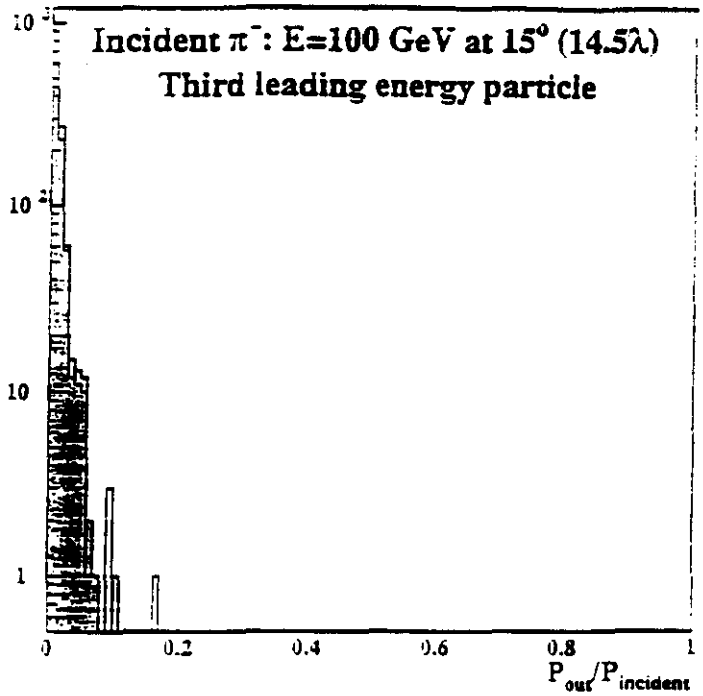

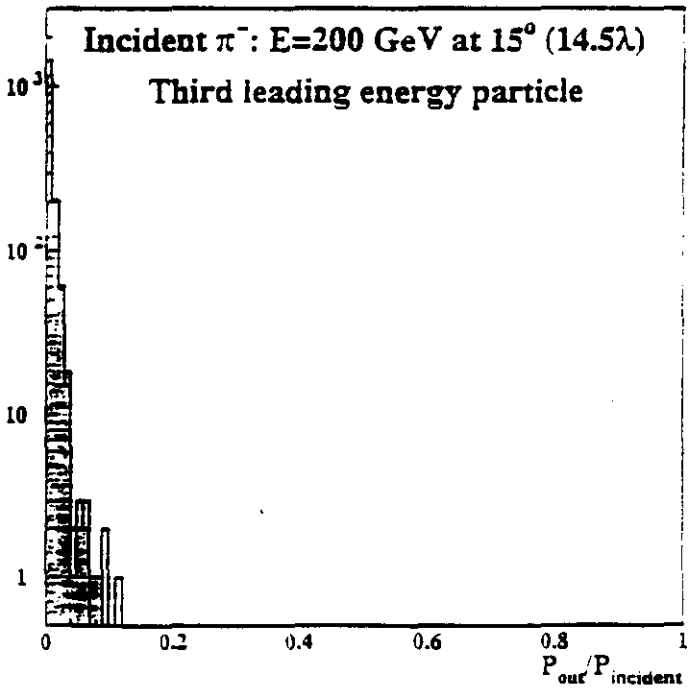

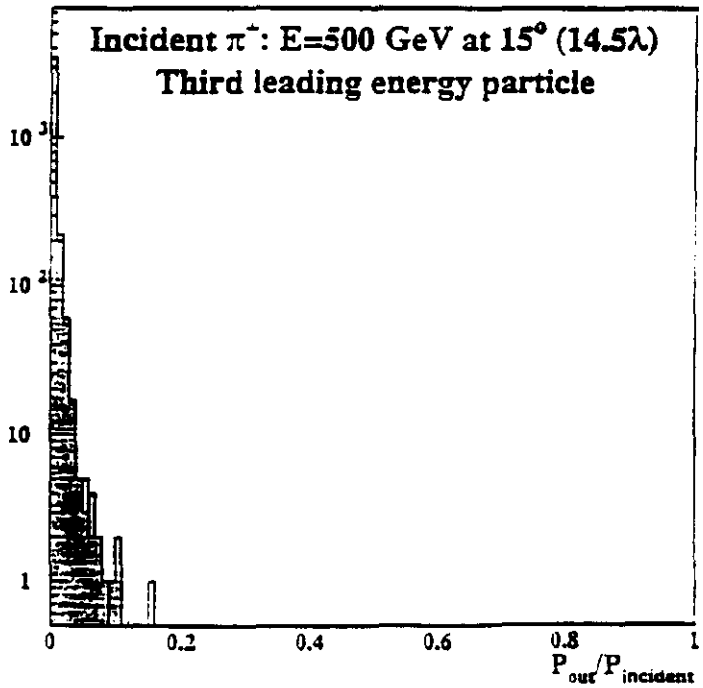

Fig. 7 continue

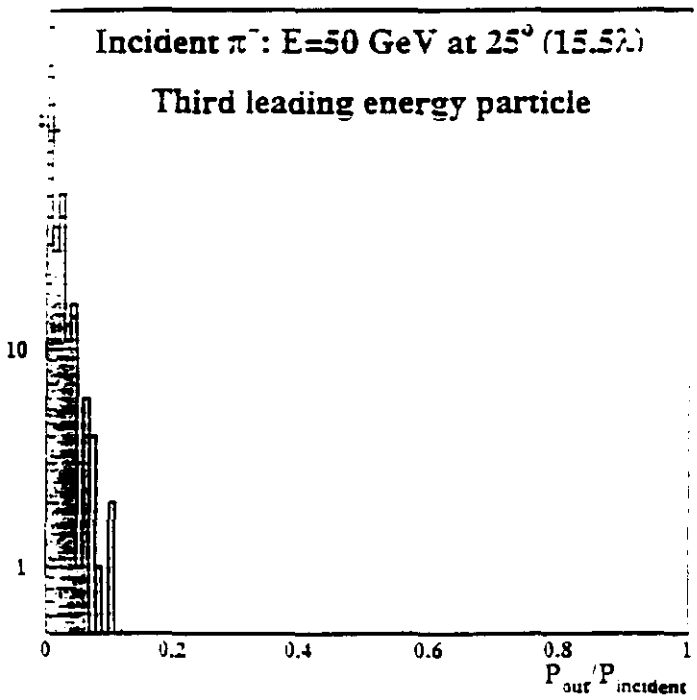

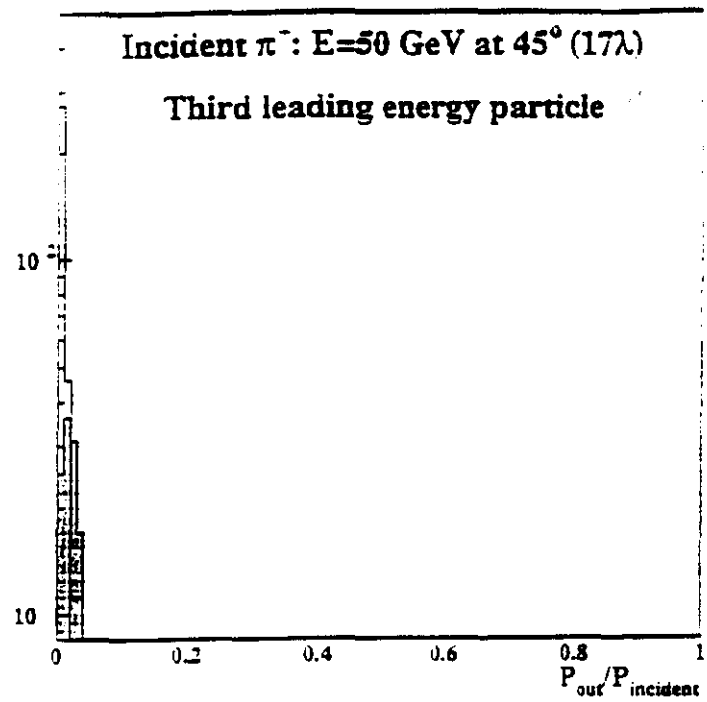

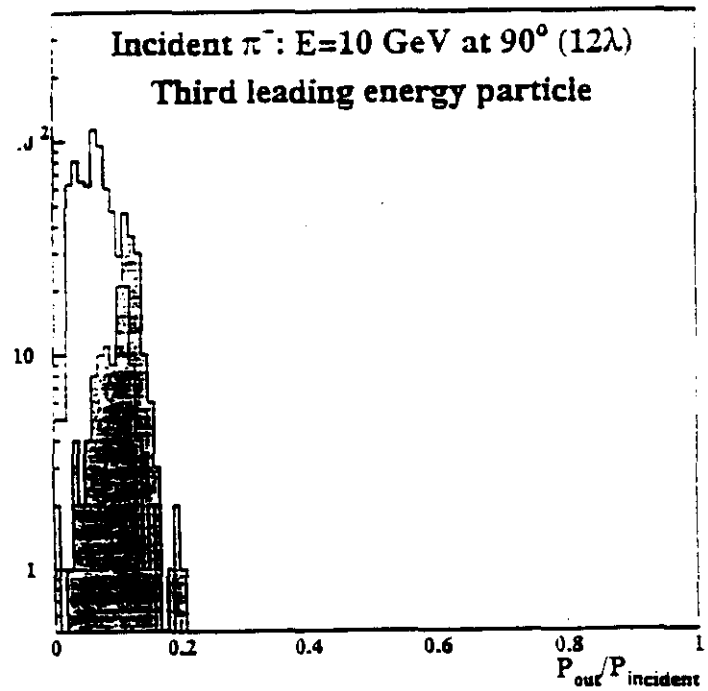

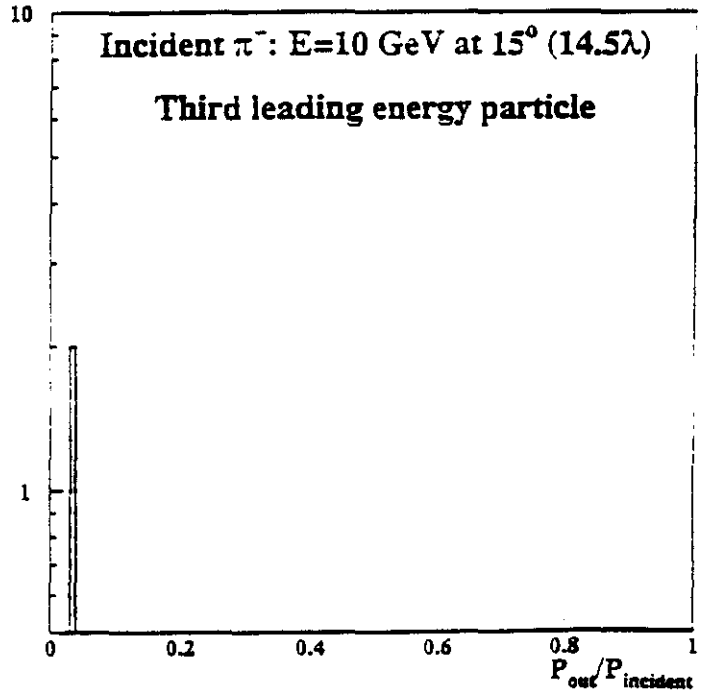

Fig. 7 continue

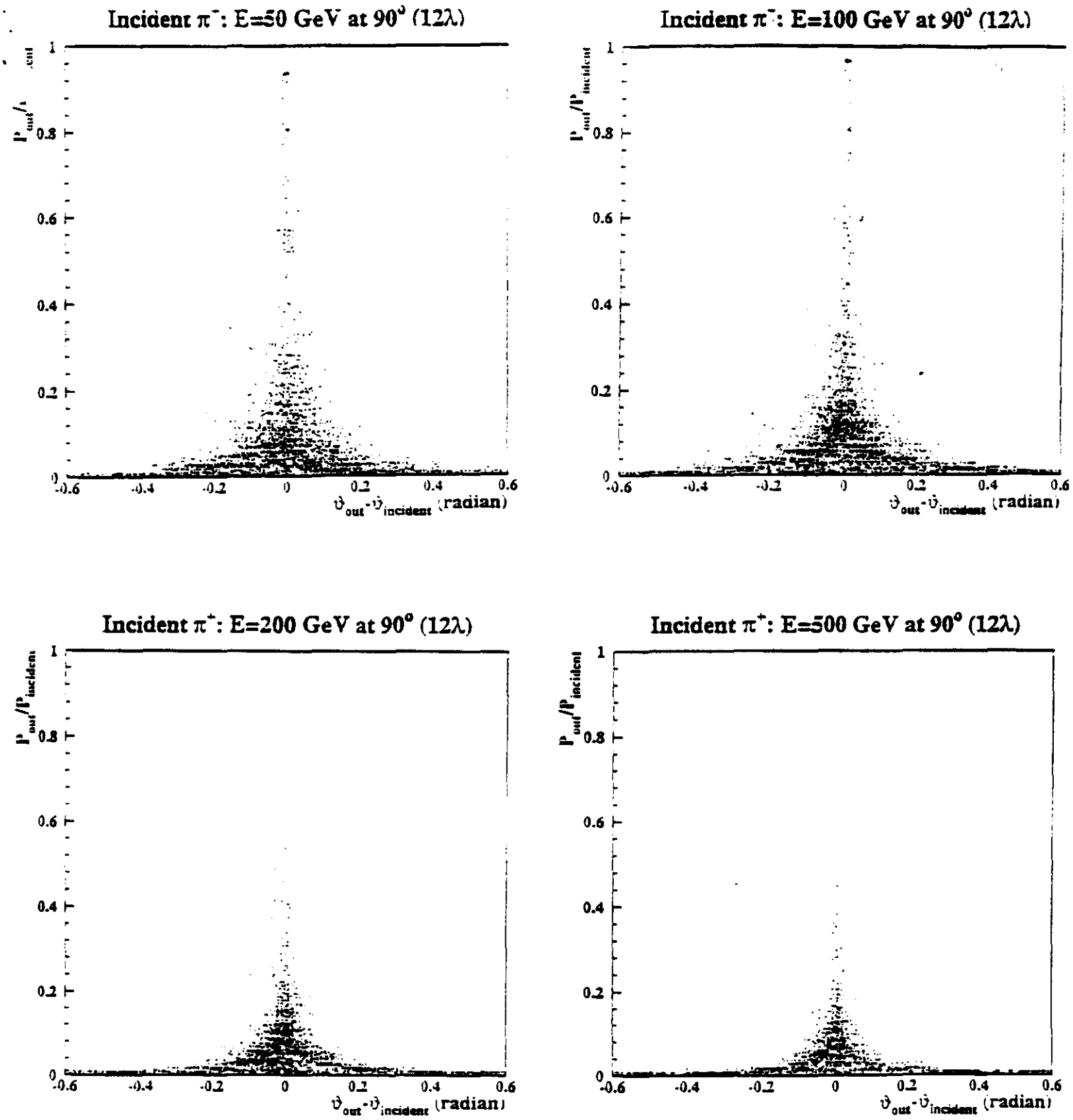

Figure 8 In total 12 figures show the punchthrough particle angular spread correlated to the normalized momentum.

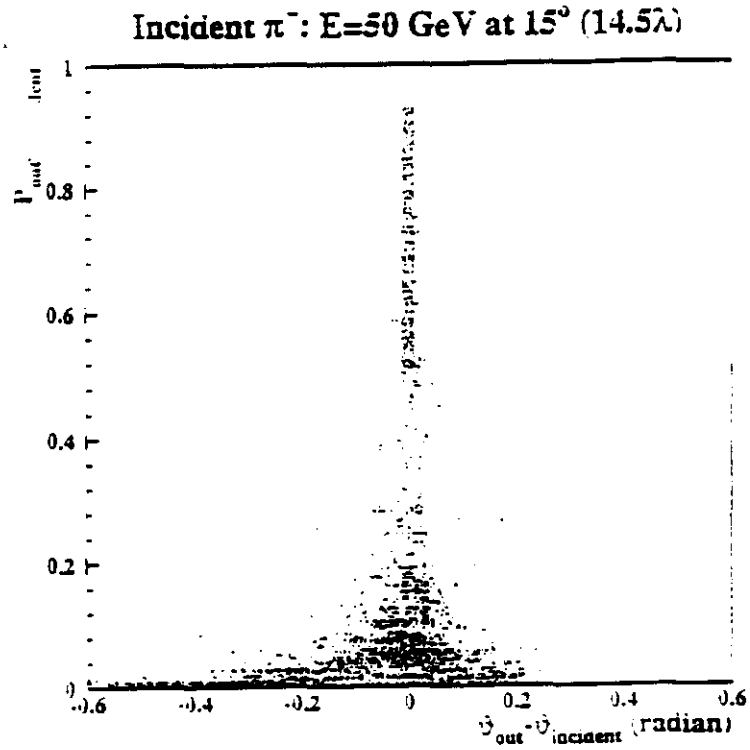

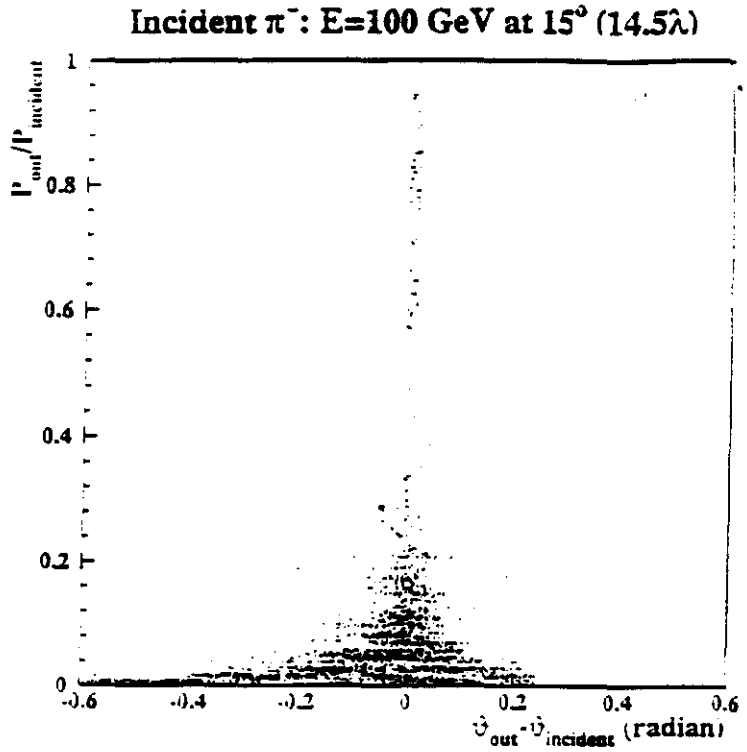

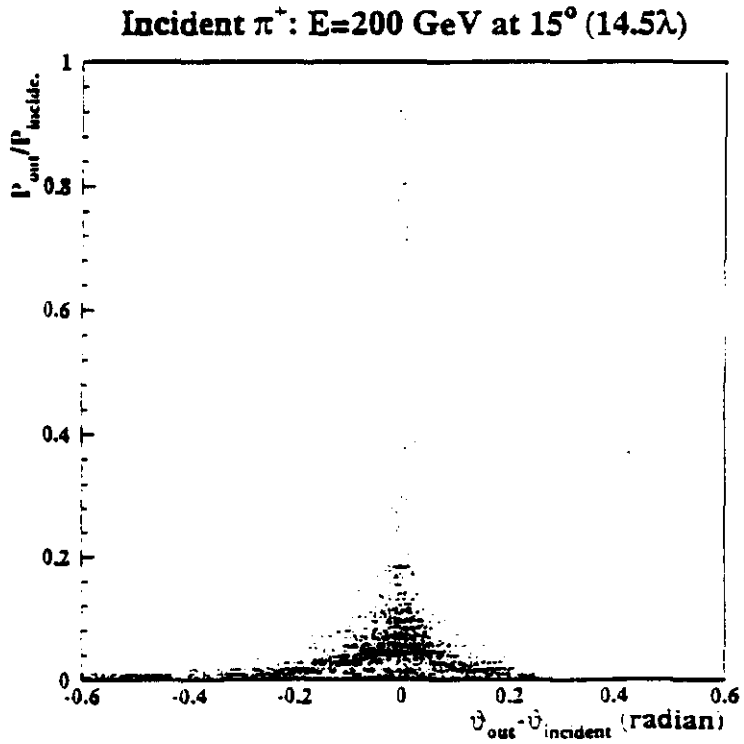

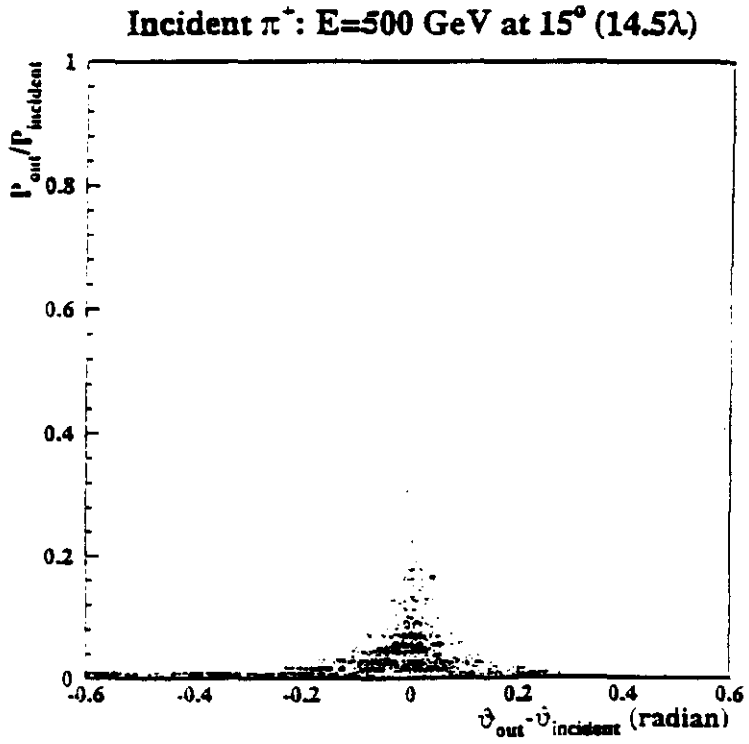

Fig. 8 continue

Incident π^-: E=50 GeV at 25° (15.5λ)

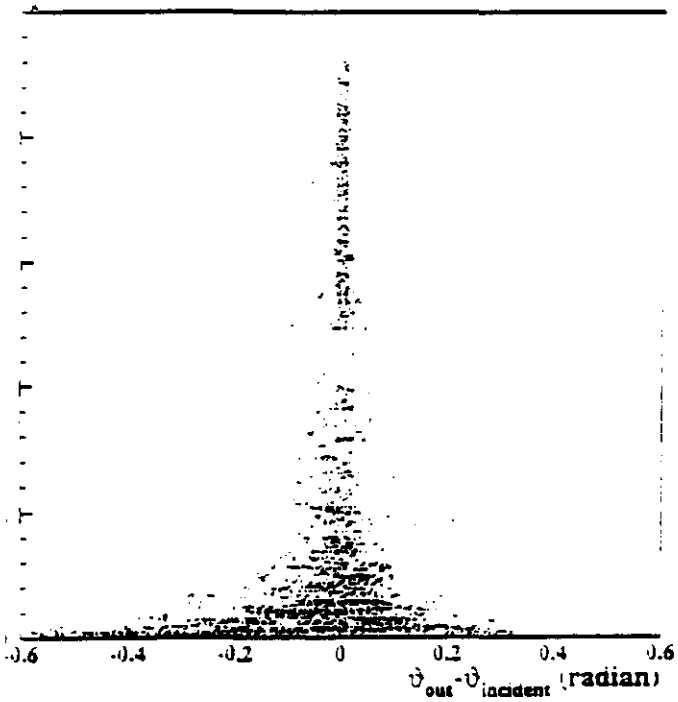

Incident π^-: E=50 GeV at 45° (17λ)

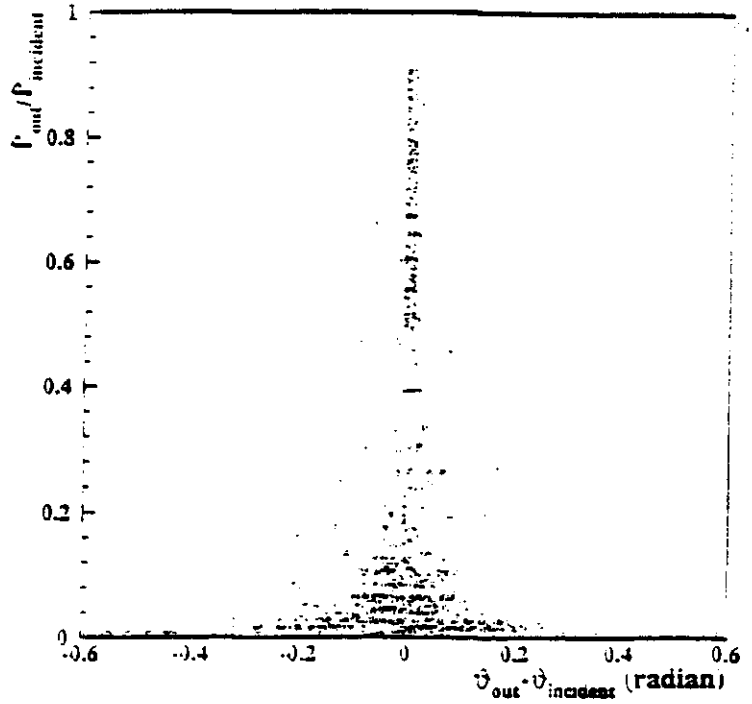

Incident π^+: E=10 GeV at 90° (12λ)

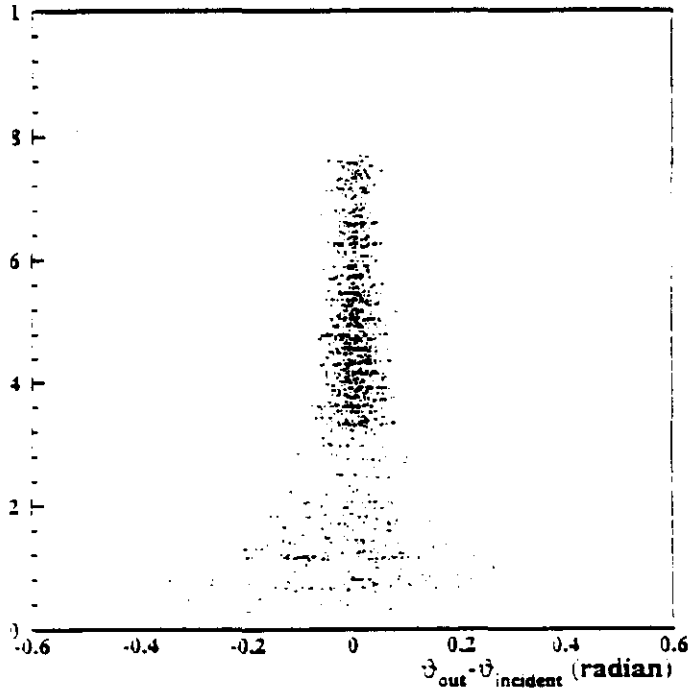

Incident π^+: E=10 GeV at 15° (14.5λ)

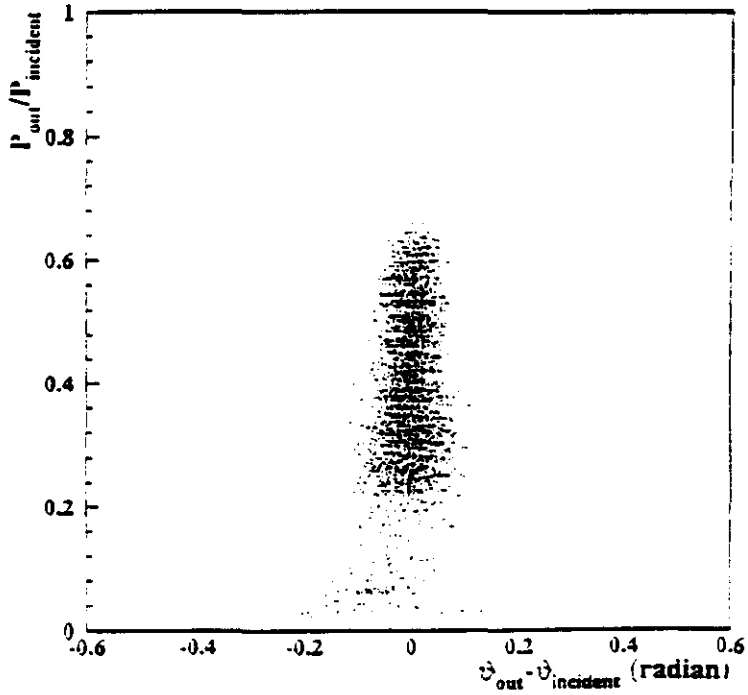

Fig. 8 continue

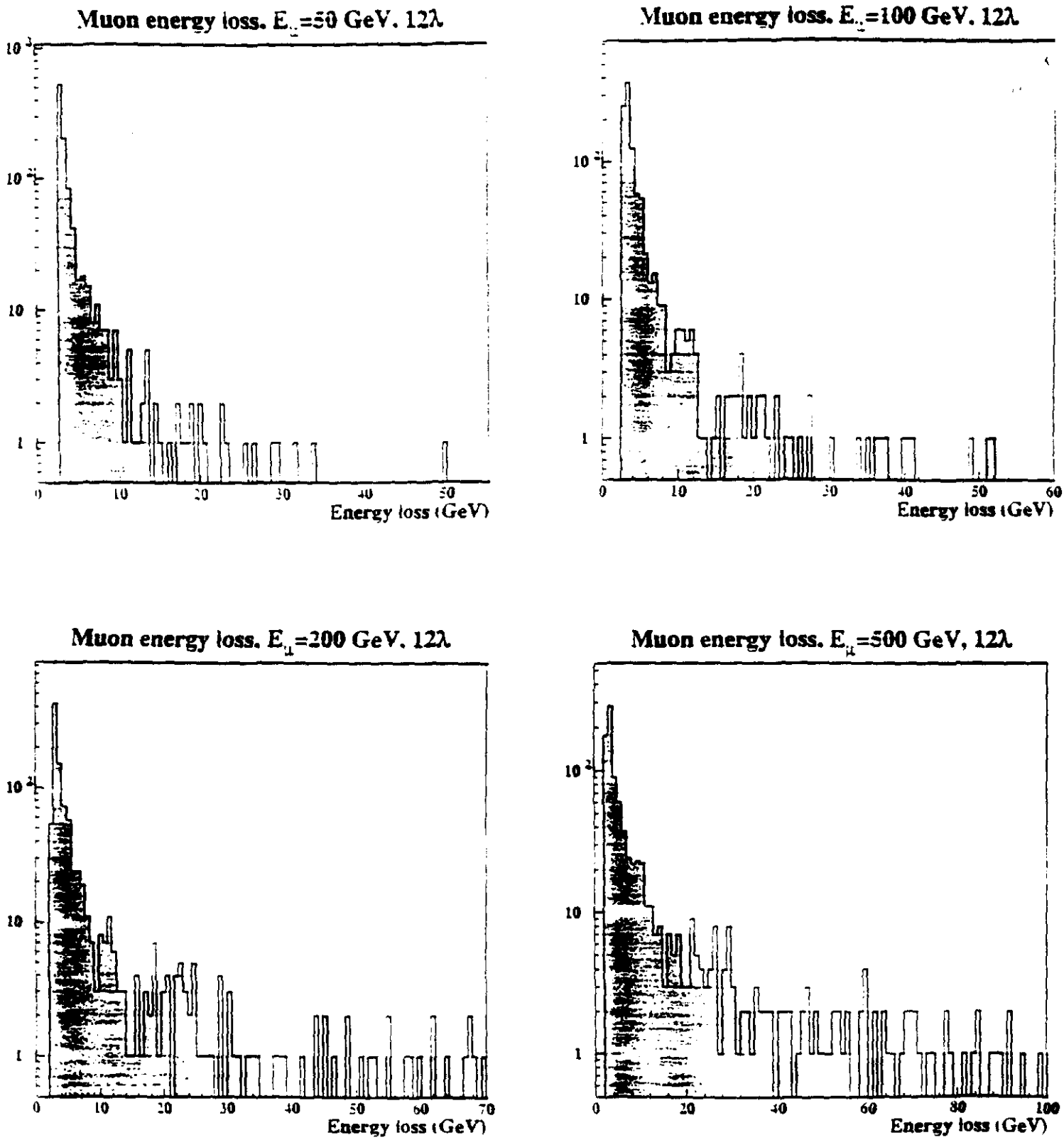

Figure 9 In total 12 figures show the muon energy loss distributions for differnt muon energies and absorber thicknesses.

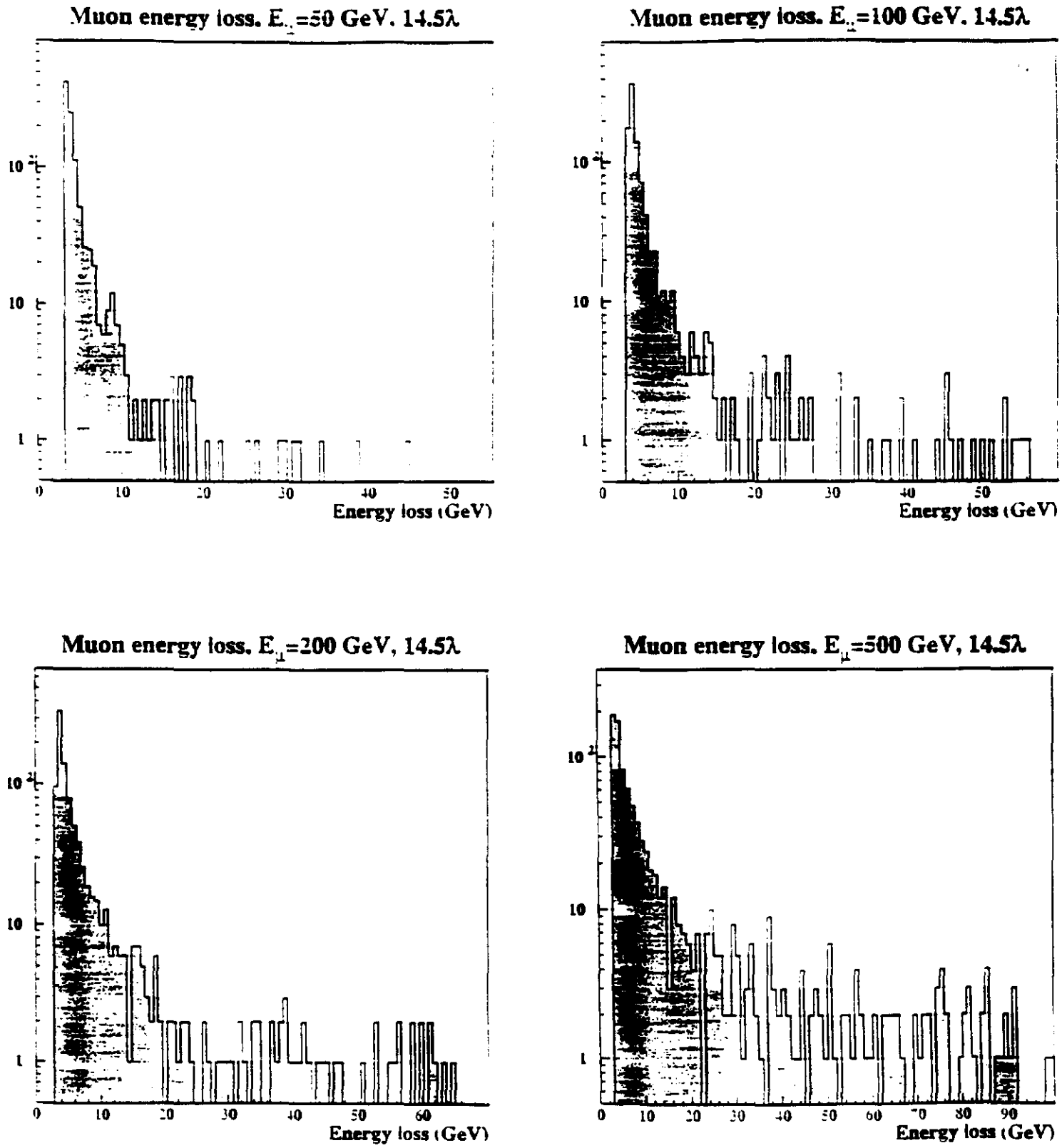

Fig. 9 Continue

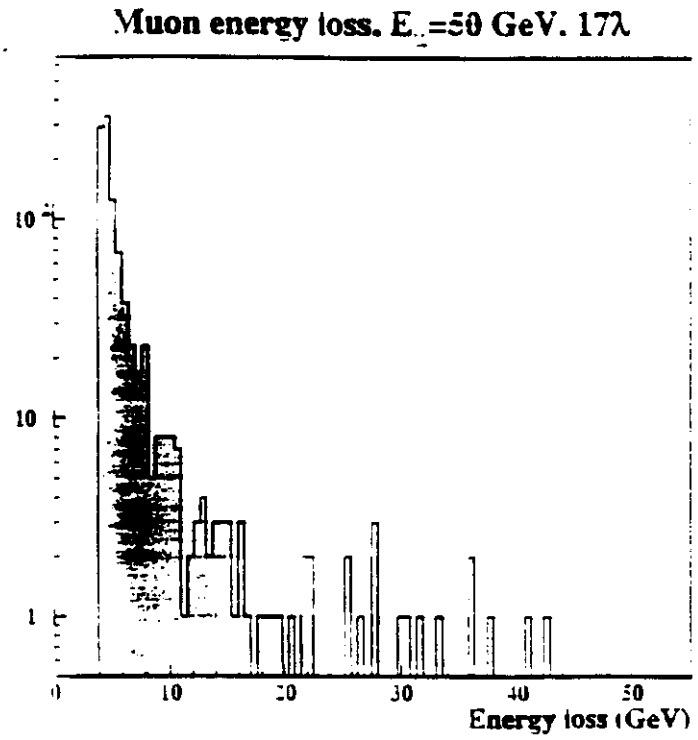

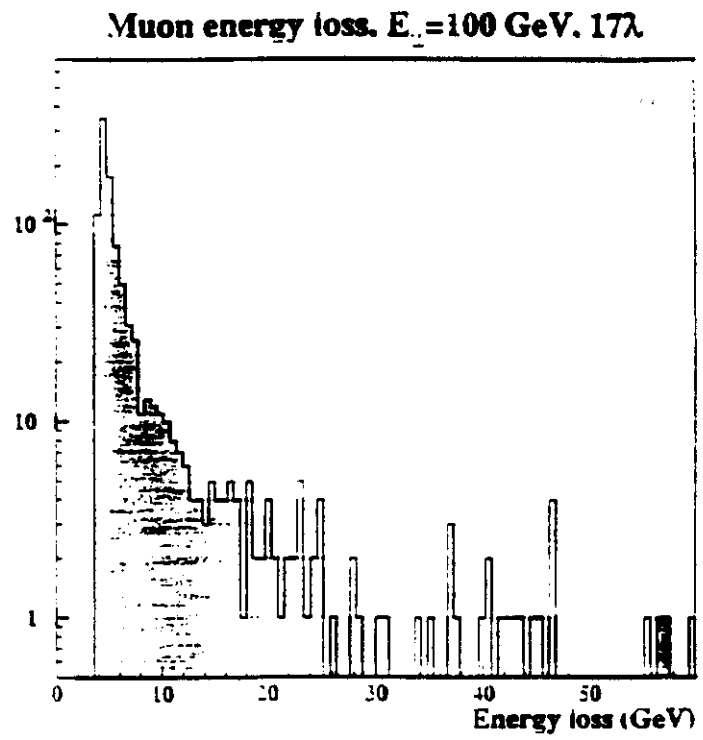

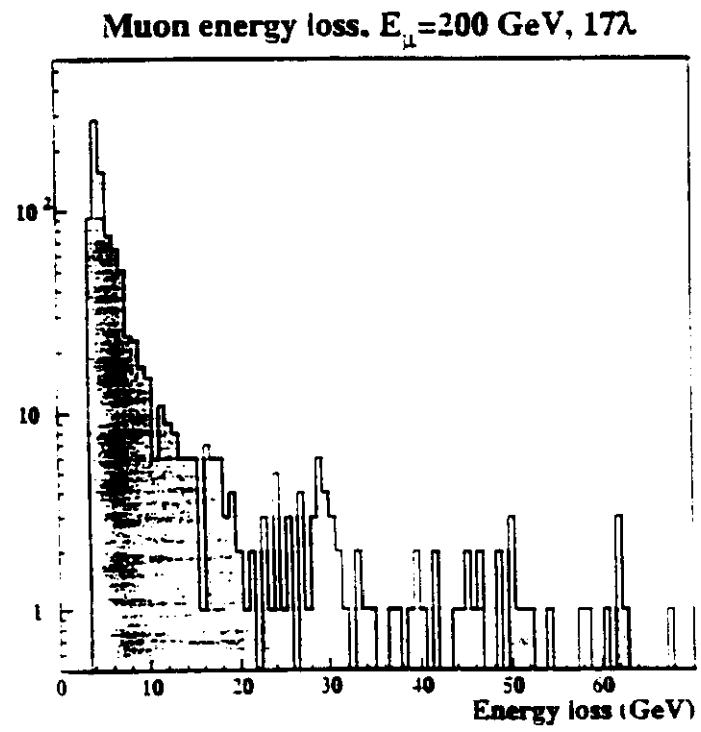

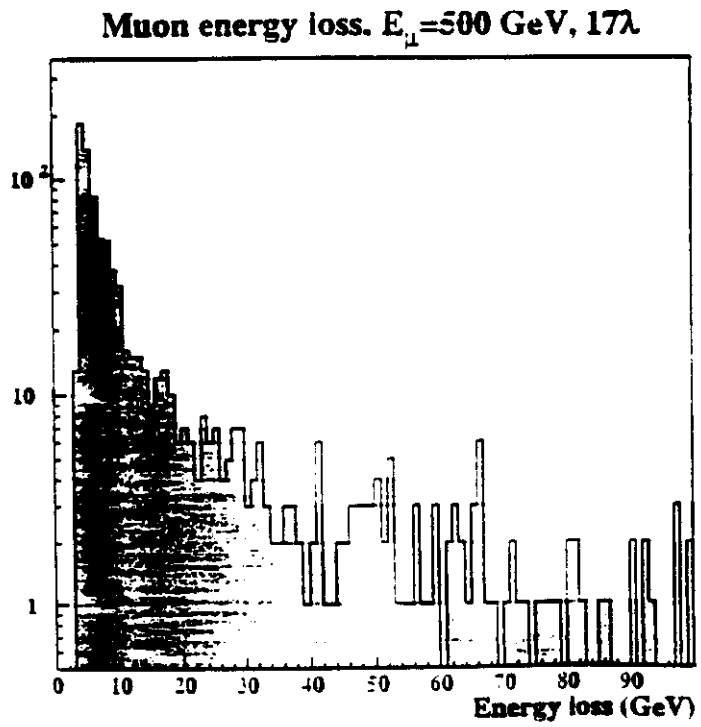

Fig. 9 continue

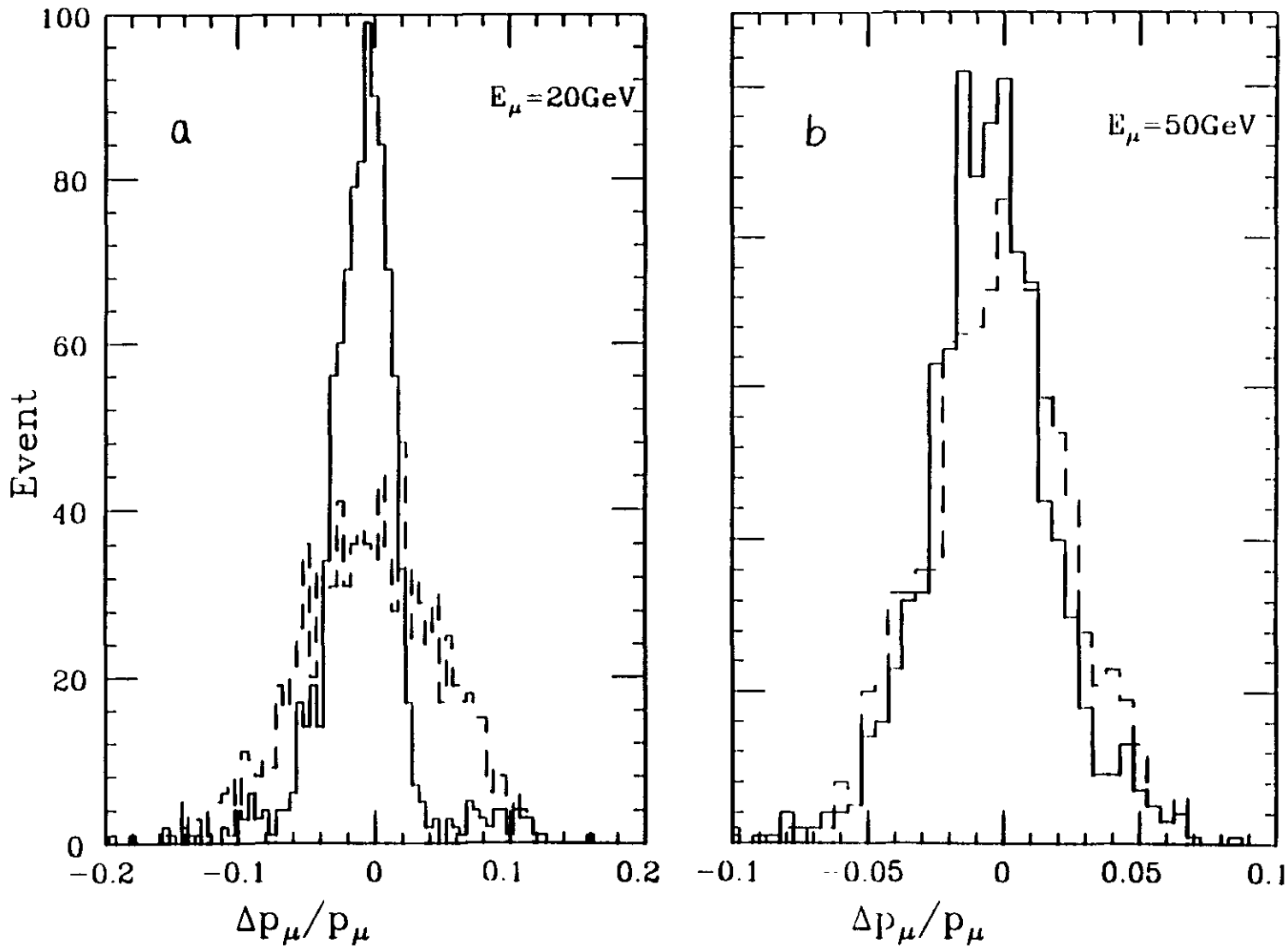

Figure 10 Muon energy resolution distributions for 20 GeV and 50 GeV muons. Solid histograms were obtained using the method described in section 3.2. Dashed histograms were obtained by adding energy loss measured in the calorimeters only.

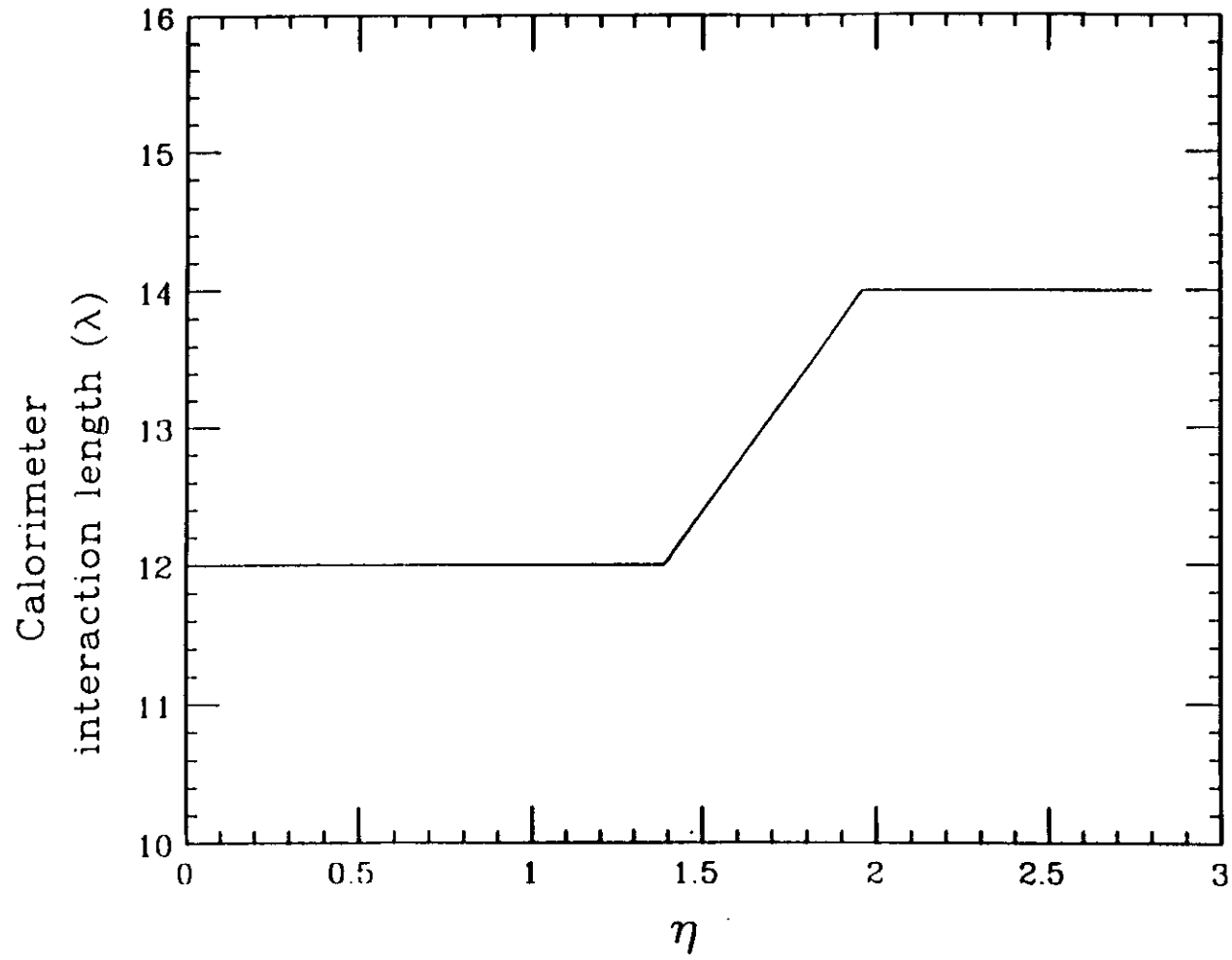

Figure 11 Calorimeter interaction length as a function of the rapidity used in our total rate calculations.

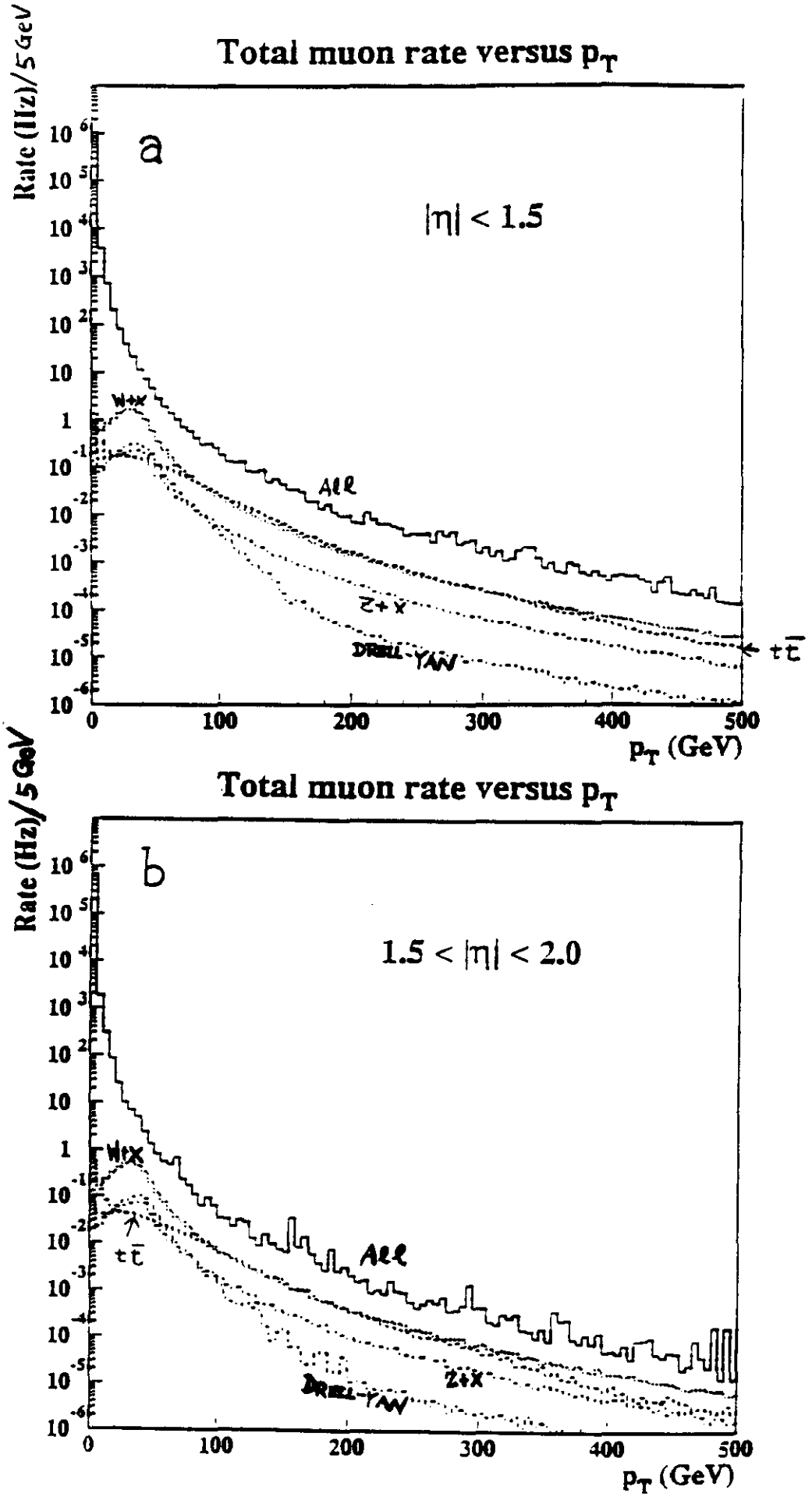
Total muon rate versus p_T
a
$|\eta| < 1.5$
Rate (Hz)/5 GeV
All
W+X
Z+X
DREL-YAN
$t\bar{t}$
p_T (GeV)
Total muon rate versus p_T
b
$1.5 < |\eta| < 2.0$
Rate (Hz)/5 GeV
All
W+X
$t\bar{t}$
Z+X
DREL-YAN
p_T (GeV)

Fig. 12

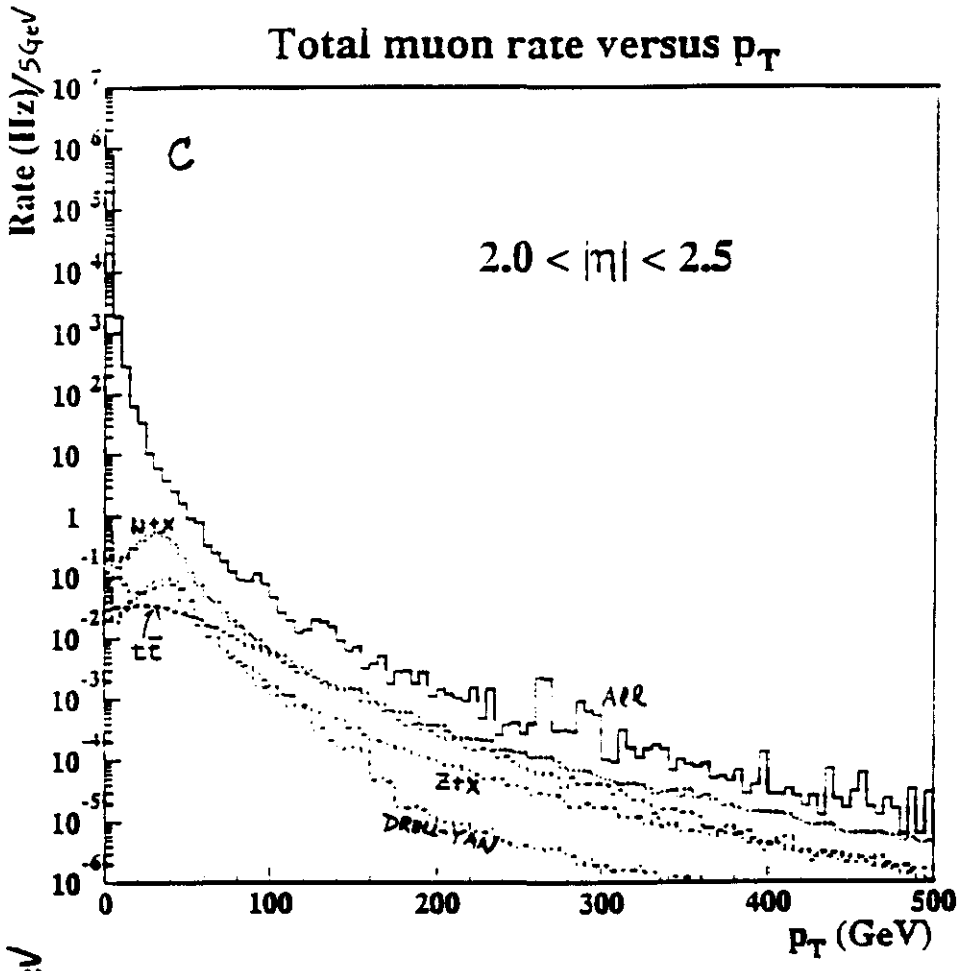

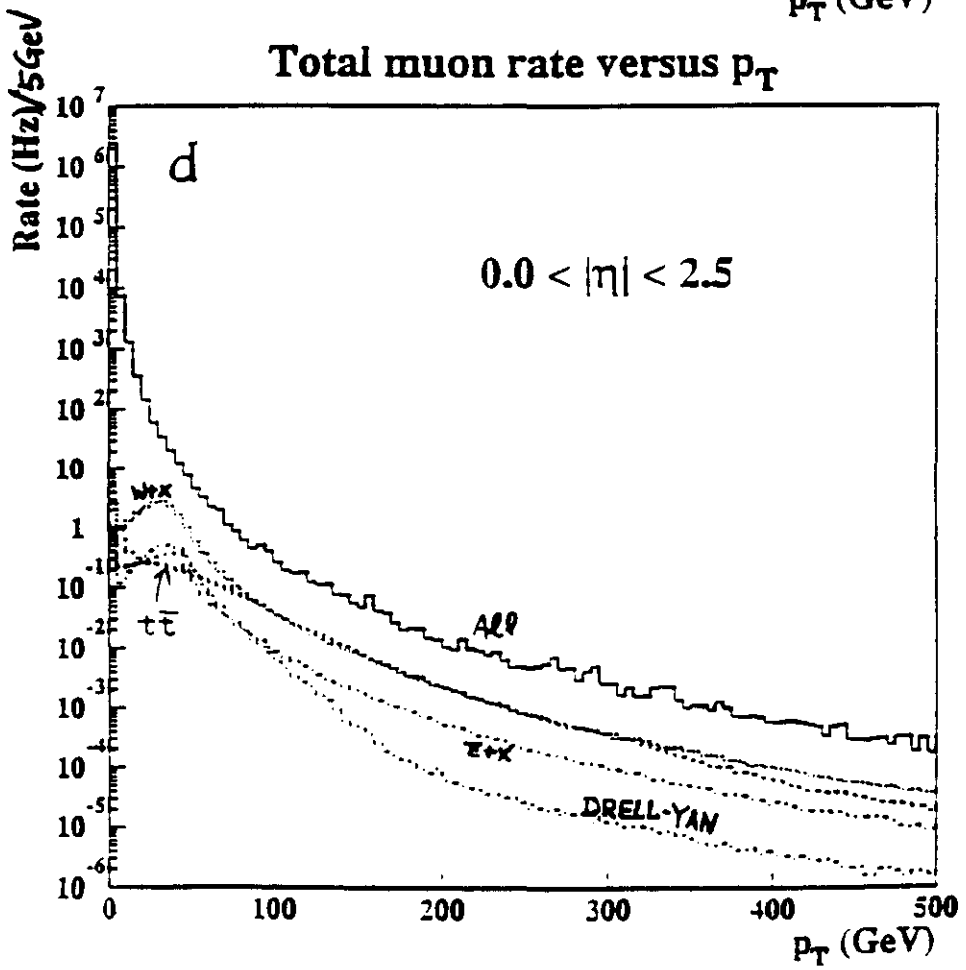

Fig. 12 continue

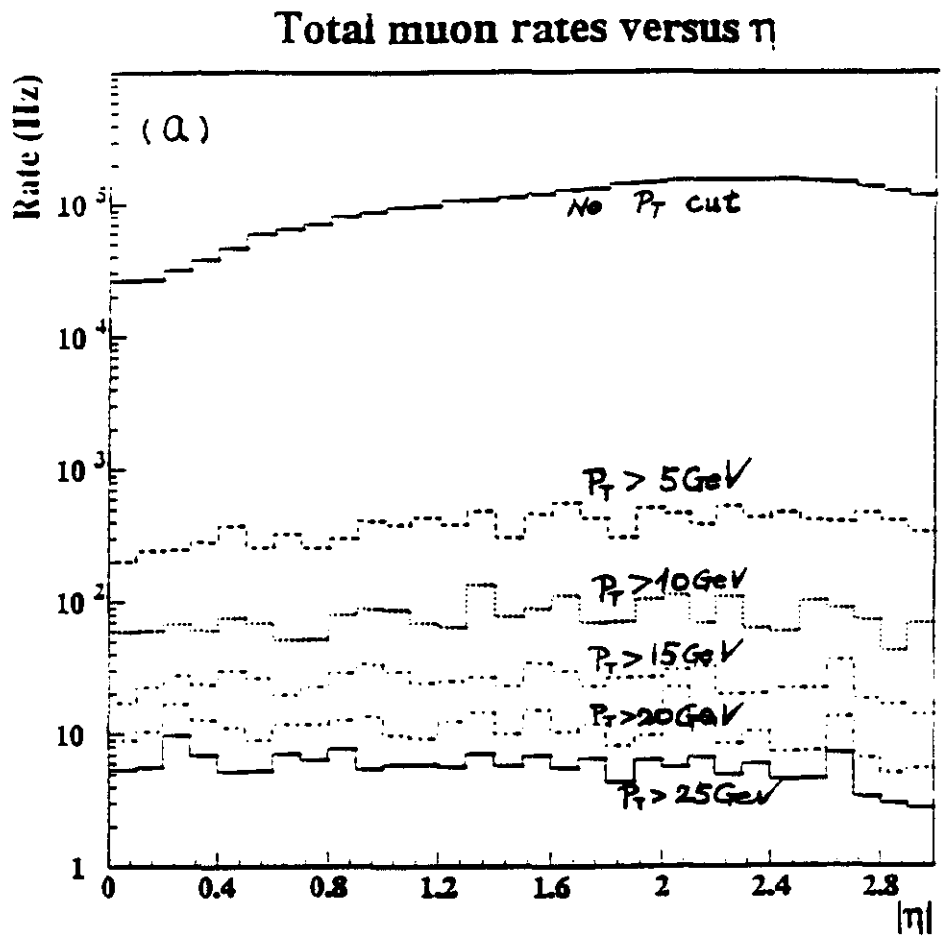
Total muon rates versus η
(a)
Rate (Hz)
No P_T cut
P_T > 5GeV
P_T > 10GeV
P_T > 15GeV
P_T > 20GeV
P_T > 25GeV
|η|

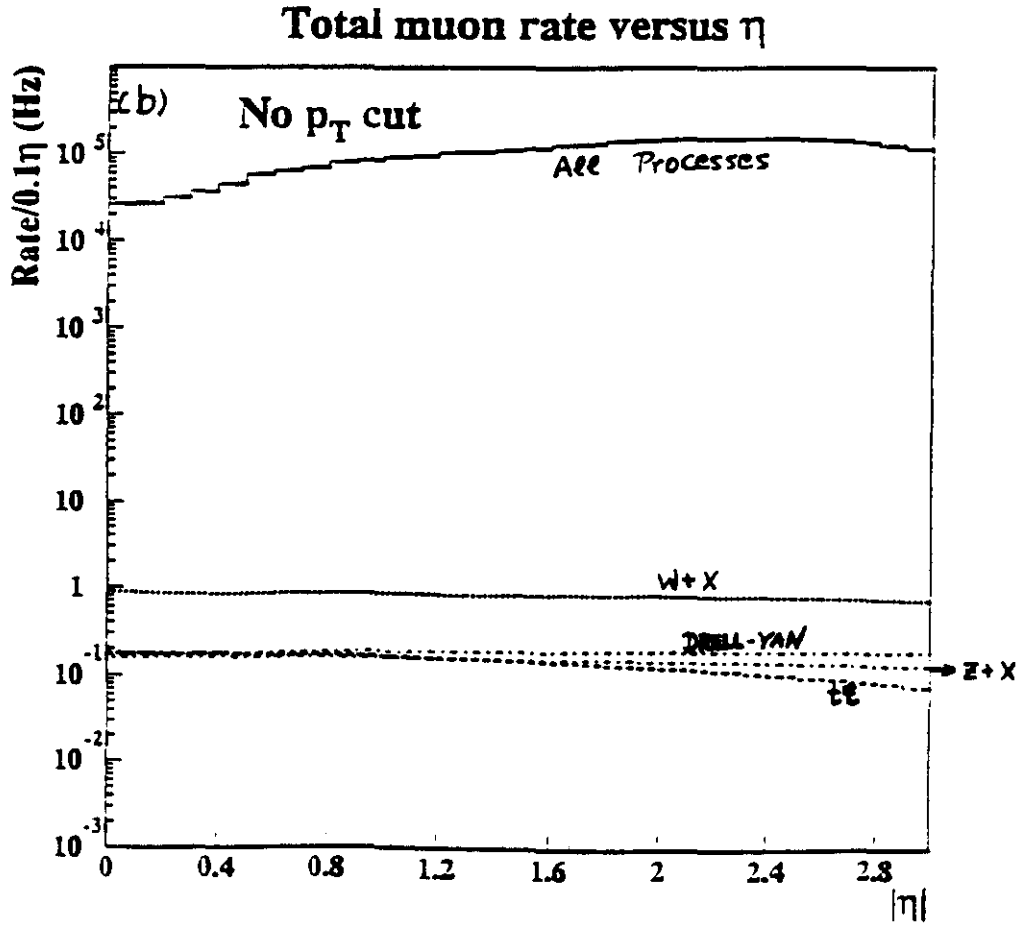
Total muon rate versus η
(b)
No p_T cut
Rate/0.1η (Hz)
All Processes
W+X
DRELL-YAN
Z+X
$t\bar{t}$
|η|

Fig. 13

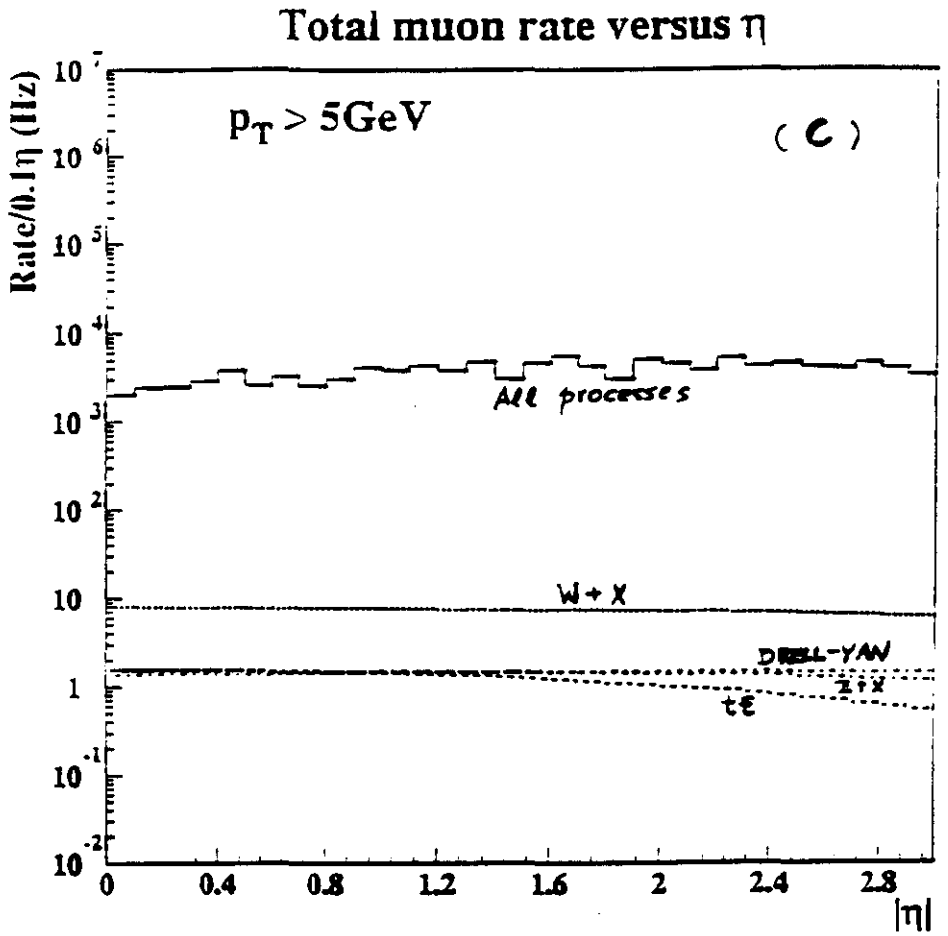

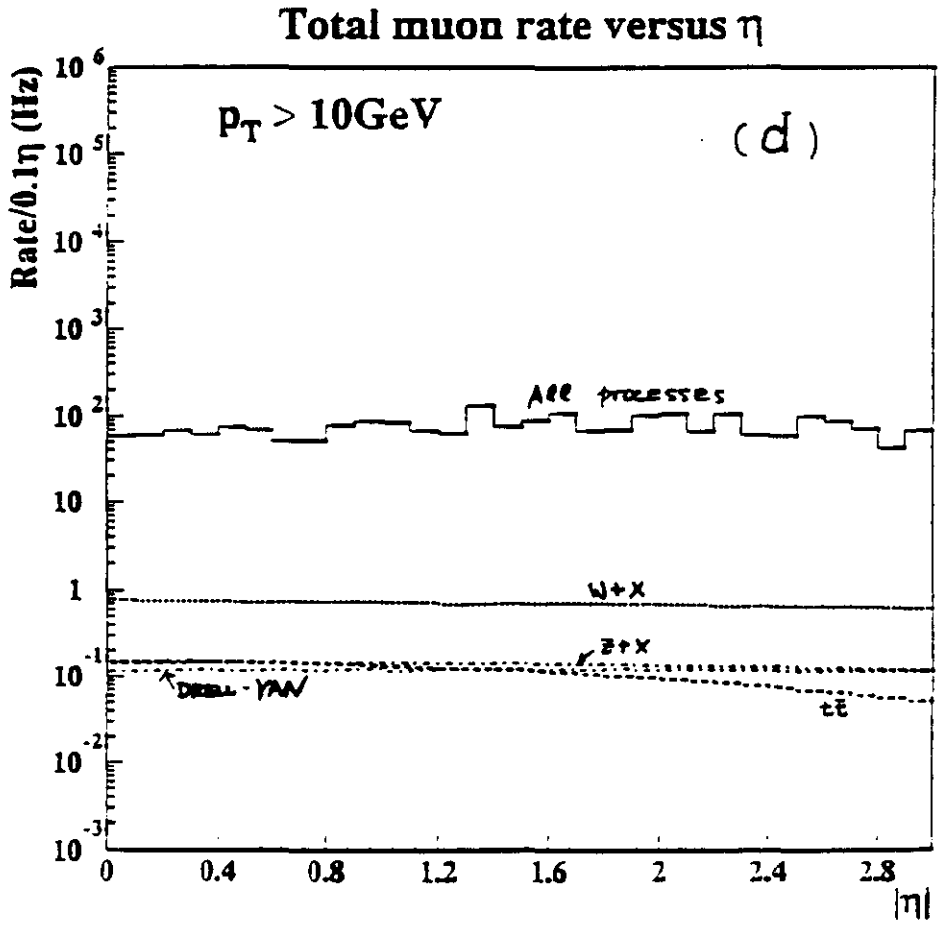

Fig. 13 continue

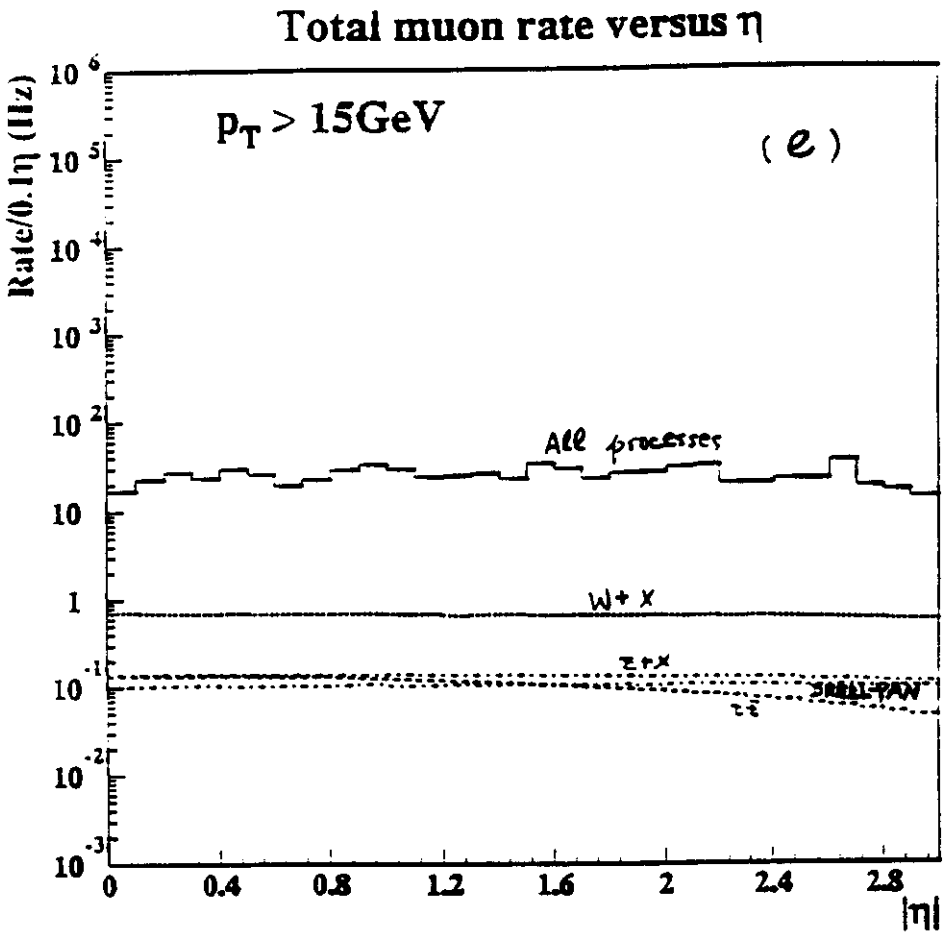

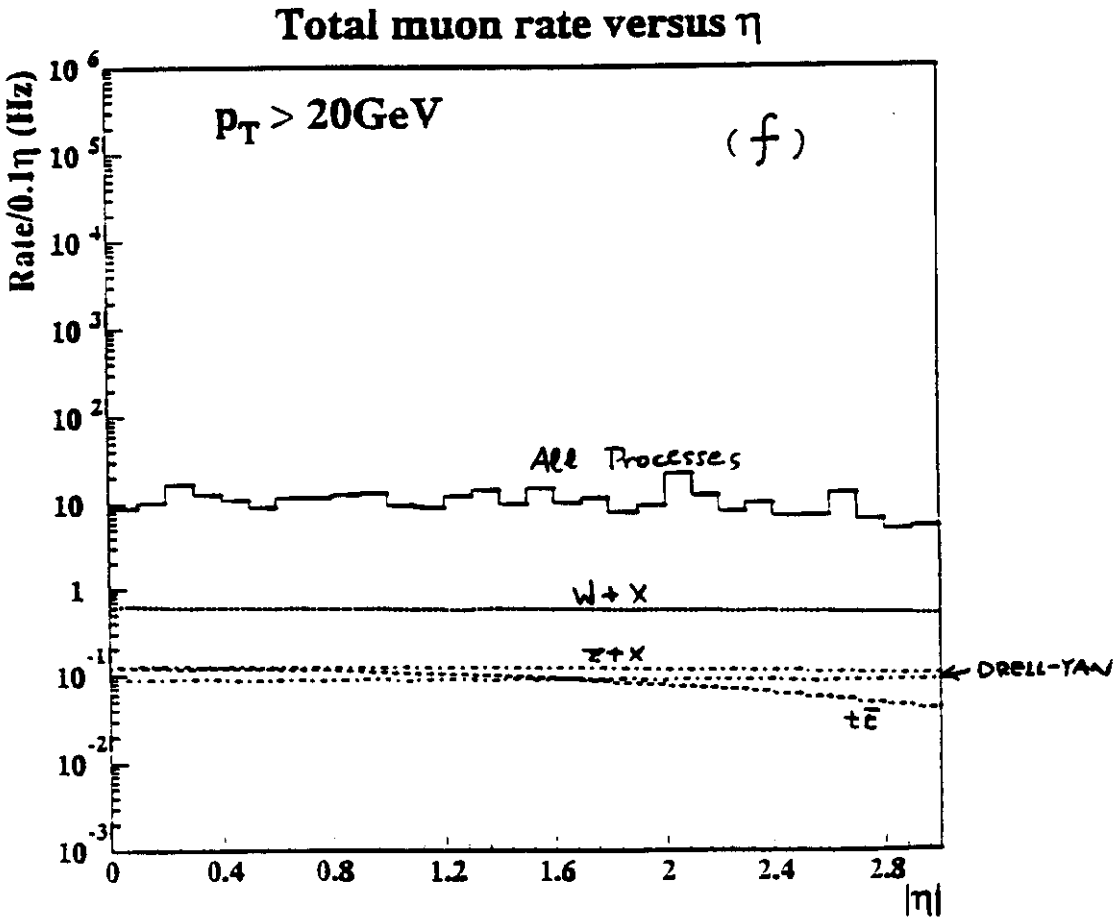

Fig. 13 continue